Homeodomain-less MEIS1 suppresses CUL3-dependent ATOH1 degradation to regulate cerebellar granule cell development

Tomoo Owa[1], Ryo Shiraishi[1], Toma Adachi[1], Satoshi Miyashita[2], Kentaro Ichijo[3], Tomoki Nishioka[4], Shinichiro Taya[1], Kozo Kaibuchi[4] and Mikio Hoshino[1*]

[1] Department of Biochemistry and Cellular Biology, National Institute of Neuroscience, NCNP, Tokyo, Japan

[2] Department of System Pathology for Neurological Disorders Brain Research Institute, Niigata University, Niigata, Japan

[3] Department of Otolaryngology and Head and Neck Surgery, Faculty of Medicine, The University of Tokyo, Tokyo, Japan

[4] Institute for Comprehensive Medical Science, Fujita Health University, Aichi, Japan

***Correspondence:** Mikio Hoshino, email address: hoshino@ncnp.go.jp

Abstract

Granule cell progenitors (GCPs) and granule cells (GCs) in the cerebellum are excellent models for studying the differentiation of neural progenitors into neurons. Although gradual degradation of ATOH1 protein in GCPs leads to their differentiation into GCs, the underlying regulatory mechanism is unclear. We show that a homeodomain-less isoform of MEIS1 (MEIS1-HdL) regulates ATOH1 degradation and GCP differentiation in a transcriptional regulation-independent manner. BMP signaling phosphorylates Ser328 of ATOH1 via ERK. CUL3 was identified as an E3-ligase that polyubiquitinates Ser328 phosphorylated ATOH1, leading to ATOH1 degradation. MEIS1-HdL and full-length MEIS1 form a trimeric complex with CUL3 and COP9 signalosome that inhibits ATOH1 ubiquitination and degradation. MEIS1-HdL is exclusively expressed in GCPs and suppresses ATOH1 degradation and GCP differentiation into GCs, despite high BMP signaling activities in the cells. Our study provides insight into the precise regulatory machinery of the degradation of the pivotal protein ATOH1 and differentiation of neural progenitors.

Introduction

Regulation of the proliferation and differentiation of neural progenitor cells into neurons is very important for development of the functional brain. Dysregulation of these processes may result in microcephaly or brain tumor. Granule cell progenitors (GCPs) and their progeny neurons, granule cells (GCs), are a good model system for studying this important developmental process. GCPs reside in the outer external GC layer (oEGL), proliferate rapidly, and then exit the cell cycle to differentiate into GCs, which successively migrate from the inner EGL (iEGL) to the inner granular cell layer(Komuro and Yacubova, 2003).

Atonal homolog 1 (ATOH1), a basic helix-loop-helix transcription factor, is involved in maintaining the proliferation and undifferentiated nature of GCPs. Loss of ATOH1 causes precocious differentiation of GCPs into GCs(Flora et al., 2009), whereas ATOH1 overexpression shows oncogenic potential in sonic hedgehog-type medulloblastoma(Ayrault et al., 2010). Thus, the level of ATOH1 protein may be precisely regulated by proteasome-dependent protein degradation. However, the underlying molecular machinery is unclear. Regarding the relevant upstream signaling pathway, bone morphogenetic protein (BMP) signaling is activated in the EGL and is involved in ATOH1 degradation in GCPs(Owa et al., 2018; Zhao et al., 2008). In colon cancer cells, WNT signaling is involved in ATOH1 degradation(Tsuchiya et al., 2007). To date, only one ubiquitin E3-ligase for ATOH1 has been identified; Forget et al. reported that HUWE1 participates in ATOH1 degradation in GCPs as the ubiquitin E3-ligase(Forget et al., 2014). However, HUWE1 was not found to be involved in BMP signaling-dependent ATOH1 degradation in GCPs, suggesting that other E3-ligases regulate ATOH1 degradation.

Myeloid ecotropic viral integration site 1 (MEIS1), a homeodomain transcription factor, is

expressed in various tissues and some tumors during development and adult stages(Schulte and Geerts, 2019). MEIS1 is involved in the maintenance of hematopoietic stem(Azcoitia et al., 2005; Hisa et al., 2004), retinal progenitor(Heine et al., 2008), and olfactory epithelial cells(Tucker et al., 2010) and is associated with acute myeloid leukemia, acute lymphoblastic leukemia(Imamura et al., 2002; Lawrence et al., 1999), and neuroblastoma(Geerts et al., 2003; Spieker et al., 2001). We previously showed that conditional deletion of the homeodomain of MEIS1 in the GC lineage resulted in a disorganized cerebellar lobular structure. In mice, the BMP signaling activities were greatly decreased, which reduced BMP-dependent ATOH1 degradation and delayed differentiation from GCPs into GCs(Owa et al., 2018). We showed that MEIS1 upregulates the transcription of Pax6, which is required for the BMP signaling activities in GCPs and GCs. However, it is unclear why ATOH1 degradation is active only in the iEGL but not in the oEGL, despite the observation that BMP signaling is strong in both these structures. In addition, the function of the homeodomain-less isoform of MEIS1 (MEIS1-HdL), which is a splicing isoform(Crist et al., 2011), is unknown.

We show that MEIS1-HdL accumulates in GCPs of the oEGL but not in GCs, whereas homeodomain-containing MEIS1 (MEIS1-FL) is distributed in both GCPs and GCs. BMP-signaling leads to phosphorylation of ATOH1-serine 328 (S328) via extracellular signal-regulated kinase (ERK). Cullin-3 (CUL3), a newly discovered ubiquitin E3 ligase for ATOH1, is involved in BMP-dependent ATOH1 degradation. CUL3 recognizes S328-phosphorylated ATOH1 (ATOH1 p-S328) and polyubiquitinates ATOH1. MEIS1-HdL and MEIS1-FL suppress BMP-dependent ATOH1 degradation by enhancing the interaction between CUL3 and constitutive photomorphogenesis 9 (COP9) signalosome, an inhibitory component of Cullin family proteins. This effect is much stronger for MEIS1-HdL than for MEIS1-FL because of their differential subcellular localization. Because MEIS1-HdL is expressed only in GCPs, BMP-dependent ATOH1-degradation is suppressed in GCPs in the oEGL, but not in GCs in the iEGL. Our study provides insight into the precise regulatory machinery involved in pivotal protein degradation and neural progenitor differentiation.

Results

MEIS1-HdL expression and localization

MEIS1-FL comprises 390 amino acids, a nuclear export sequence, and a nuclear localizing signal. MEIS1-HdL comprises 251 amino acids and has a nuclear export sequence (Figure 1A). We collected the GCP-enriched fraction from the P6 cerebellum, which contains mostly GCPs, with little contamination by GCs(Adachi et al., 2021). RT-PCR revealed that GCPs strongly expressed MEIS1-FL and weakly expressed MEIS1-HdL transcripts (Figure 1B), which was confirmed with immunoblotting (Figure 1C).

We utilized two groups of knock-in mice expressing one of the following two fusion proteins:

ATOH1-GFP, a marker of ATOH1-expressing GCPs, or Ki67-RFP, a marker of GCPs (Figure1—figure supplement 1A–C). Fluorescence-activated cell sorting of the GCP-enriched fraction was performed to purify ATOH1-expressing GCPs, (GFP^+, RFP^+), ATOH1-nonexpressing GCPs, (GFP^-, RFP^+), and GCs (GFP^-, RFP^-) (Figure 1D, Figure1—figure supplement 1D, E). Quantitative reverse transcription polymerase chain reaction (qRT-PCR) revealed that MEIS1-HdL was enriched in ATOH1-expressing GCPs and only minimally expressed in ATOH1-nonexpressing GCPs or GCs. In contrast, MEIS1-FL was evenly expressed in all cell types (Figure 1E). This implies that MEIS1-HdL has a specific function in ATOH1-expressing GCPs.

To investigate MEIS1-FL and MEIS1-HdL intracellular localization, we transfected them into Neuro2a (N2a) cells and performed subcellular fractionation and immunoblotting. MEIS1-FL was detected very strongly in the nuclear fraction and moderately in the cytoplasmic fraction, whereas MEIS1-HdL was detected exclusively in the cytoplasmic fraction (Figure 1F). Immunocytochemistry using MEIS1-FL-EGFP or MEIS1-HdL-EGFP fusion protein transfected into N2a cells showed similar findings (Figure 1G, H). Predominantly cytoplasmic localization of MEIS1-HdL has been reported in other cell types(Crist et al., 2011) and is perhaps attributed to the lack of a nuclear-localizing signal in this isoform (Figure 1A).

Roles of MEIS1 isoforms in GCP and GC development

To examine how the MEIS1 isoforms affect GC development, we introduced an expression vector for each isoform into GCPs facing the pia mater (ATOH1-expressing GCPs) via electroporation into the P8 cerebella. At 72 h after electroporation (P11), electroporated animals were fixed and immunostained. Electroporated-cell nuclei were visualized using co-electroporated histone H3.1-GFP. In the control group, the electroporated cells (GFP^+ cells) comprised approximately 50% GCPs ($Ki67^+$ cells, Figure 2A, D) and 50% GCs ($p27^+$ cells; Figure 2E, Figure2—figure supplement 1A).

MEIS1-FL overexpression decreased GCP counts and increased GC counts, whereas the opposite trend was observed when MEIS1-HdL was overexpressed (Figure 2B–E, Figure2—figure supplement 1B, C). This result suggests that the proteins have contrasting roles in GC differentiation from GCPs, with MEIS1-HdL exerting suppressive effects and MEIS1-FL accelerating differentiation. A similar tendency was observed for ATOH1-expressing GCPs (Figure 2A–C, F). This promotion of GCP differentiation by MEIS1-FL is consistent with our previous observation that MEIS1 differentiates GCPs by upregulating BMP signaling(Owa et al., 2018).

To elucidate the physiological function of MEIS1-HdL, we generated an MEIS1-HdL knockdown vector (sh-*Meis1*-HdL) that suppressed the expression of MEIS1-HdL but not MEIS1-FL (Figure3—figure supplement 1A). In contrast, the knock-down vector used previously (sh-*Meis1*-all)(Owa et al., 2018) suppressed both MEIS1-FL and MEIS1-HdL (Figure3—figure

supplement 1A, right panel). Using these vectors and histone H3.1-GFP, we electroporated the cerebella at P8; 72 h after electroporation, we immunostained the cerebellar sections at P11. *Meis1*-HdL-knockdown reduced the ratio of mitotic cells (GCPs; Figure 3A, D) and increased that of postmitotic cells (GCs; Figure 3E, Figure3—figure supplement 1B). Similar tendency was observed for ATOH1-expressing GCPs. These effects were rescued by co-electroporation with the knockdown-resistant Meis1-HdL expression vector (Res-Meis1-HdL) (Figure 3B, D, E, F, Figure3—figure supplement 1C). These findings suggest that MEIS1-HdL participates in suppressing GCP differentiation into GCs. Interestingly, electroporation of sh-*Meis1*-all did not significantly alter the proportion of GCPs (Figure 3C, D) or GCs (Figure 3E, Figure3—figure supplement 1D), although it caused a subtle but significant reduction in ATOH1-expressing GCPs (Figure 3C, F). We expect that this was caused by the suppression of both isoforms.

MEIS1 stabilizes the level of ATOH1

Controlling the ATOH1 protein amount is important to regulate GCP differentiation into GCs(Ayrault et al., 2010; Helms et al., 2001; Miyashita et al., 2021). Given that MEIS1-HdL suppresses this differentiation, MEIS1 might participate in regulating ATOH1 levels. To test this, we measured ATOH1 fluorescence intensity in cerebella electroporated with *sh-Meis1* at P8 and fixed at P11. As expected, among ATOH1-expressing GCPs located on the pial side of the EGL, fluorescence intensities were lower in sh-*Meis1*-HdL-transfected cells (GFP^+ cells, arrows in Figure3—figure supplement 2A–C) than in surrounding non-electroporated cells (GFP^- cells, arrowheads in Figure3––figure supplement 2A–C) (Figure3—figure supplement 2E). In contrast, *sh-Meis1-HdL* introduction did not affect Ki67 fluorescence intensity. This suggests that MEIS1 may participate in maintaining ATOH1 protein in ATOH1-expressing GCPs. Similar results were observed following *sh-Meis1-all* introduction (Figure3—figure supplement 2C–E).

Next, we transfected Atoh1 and Meis1 expression vectors into N2a cells and performed immunoblotting. We used a GST-tagged ATOH1 (GST-ATOH1) expression vector to discriminate between endogenous and exogenous ATOH1 protein, although it is known that N2a cells do not express endogenous ATOH1 under normal conditions(Wu et al., 2013). Administration of MG132, an inhibitor of proteasome-dependent protein degradation, enhanced the ATOH1 signals (lane 5, Figure 4A) relative to the control (lane 1), consistent with the previous finding that ATOH1 is degraded via proteasome-dependent protein degradation(Cheng et al., 2016; Forget et al., 2014; Zhao et al., 2008). Interestingly, ATOH1 signals were also higher following co-transfection with MEIS1-HdL (lane 3 in Figure 4A) or MEIS1-FL (lane 4), whereas the N-terminal MEIS1 fragment (1–130 aa) did not exhibit such an effect (lane 2). To further analyze ATOH1 stability, we immunoblotted transfected N2a cells treated with cycloheximide for 0, 4, and 8 h. This revealed that MEIS1-HdL and MEIS1-FL both strongly suppressed ATOH1 degradation, to the same extent as

MG132 administration (Figure 4B, C).

MEIS1 inhibits the interaction between CUL3 and ATOH1

We attempted to estimate ATOH1 ubiquitination in cultured cells. N2a cells were co-transfected with GST-ATOH1 and HA-Ub and cultured with MG132 to block proteasome-dependent protein degradation. Then, GST-ATOH1 was pulled down by glutathione-beads and immunoblotted with an anti-HA antibody. Consistent with previous findings(Cheng et al., 2016; Forget et al., 2014), ATOH1 was strongly polyubiquitinated (Figure 5A, lane 1). However, co-transfection with MEIS1-FL or MEIS1-HdL significantly reduced GST-ATOH1 polyubiquitination (Figure 5A, lanes 2, 3, 5B). Interestingly, MEIS1-HdL suppressed polyubiquitination more strongly than MEIS1-FL (Figure 5B). These findings suggest that these MEIS1 isoforms suppress the functions of molecules related to ATOH1 polyubiquitination, eventually blocking ATOH1 degradation. The fact that both MEIS1-FL and MEIS1-HdL do this suggests that this function is not elicited by MEIS1-induced transcriptional regulation.

Based on our evidence suggesting that MEIS1 isoform proteins affect the function of molecules involved in protein ubiquitination, we searched for ATOH1-binding molecules in cultured cells. After transfecting GST-ATOH1 or GST-ATOH1 plus MEIS1 into N2a cells, GST-ATOH1 was pulled down, and its binding molecules were subjected to LC–MS/MS (Figure 5C). We obtained many candidate molecules that bind ATOH1 in the presence or absence of MEIS1 (see Supplementary File). We identified several molecules (Figure 5D) that bind ATOH1 only in the absence of MEIS1 (Figure 5D). CUL3 is known to form a complex with UBE2M and acts as an E3-ligase; its activity is regulated by the binding of CAND1(Baek et al., 2021; Chua et al., 2011; Petroski and Deshaies, 2005). To date, HUWE1 is the only E3-ligase reported to participate in ATOH1 degradation. Although we found that HUWE1 binds to GST-ATOH1, its binding ability was not affected by MEIS1.

To confirm the binding of ATOH1 and MEIS1, we co-transfected GST-ATOH1 and MEIS1-FL or MEIS1-HdL into N2a cells, followed by pull-down with GST-ATOH1 and immunoblotting with a CUL3 antibody. Consistent with the LC–MS/MS results, CUL3 bound ATOH1 in the absence of MEIS1 (Figure 5E, lane 1), but not following co-transfection with MEIS1-FL or MEIS1-HdL (lanes 2, 3). Next, we examined the involvement of CUL3 in ATOH1 polyubiquitination. GST-ATOH1 and HA-Ub were co-transfected with a control or *Cul3*-knockdown vector (sh-*Cul3*) into N2a cells, which were subjected to pulldown and immunoblotting with the indicated antibodies (Figure 5F), in the absence of MG132. GST-ATOH1 polyubiquitination was strongly suppressed by *Cul3*-knockdown (Figure 5F), suggesting that CUL3 participates in ATOH1 polyubiquitination. To further analyze the effect of *Cul3*-knockdown on ATOH1 stability, we immunoblotted N2a cells transfected with GST-ATOH1 and control or sh-*Cul3* and administered cycloheximide for 0, 4, and 8

h (Figure 5G). This revealed that *Cul3*-knockdown markedly suppressed ATOH1 degradation in N2a cells (Figure 5H).

BMP-dependent ATOH1 degradation mediated by the ERK-CUL3 pathway.

Previous studies showed that phosphorylation of ATOH1 regulates its degradation(Cheng et al., 2016; Forget et al., 2014; Tsuchiya et al., 2007). Hence, we hypothesized that MEIS1 affected ATOH1 phosphorylation. Using N2a cells transfected with Atoh1 alone or Atoh1 and Meis1-FL, we investigated the ATOH1 phosphorylation sites using LS–MS/MS (Figure5—figure supplement 1A). We found that ATOH1 phosphorylation was increased in the presence of MEIS1-FL (see Supplementary File). Particularly, S328 phosphorylation was greatly increased (Figure5—figure supplement 1B). Immunoblotting analysis using an antibody against ATOH1 p-S328 revealed that it accumulated in the presence of MEIS1-FL and MEIS1-HdL (Figure5—figure supplement 1C).

S328 phosphorylation was reported to be involved in the degradation of ATOH1(Cheng et al., 2016; Forget et al., 2014). Accordingly, the cycloheximide (Chx) chase assay showed that ATOH1-S328A (Ser 328 of ATOH1 was replaced with Ala; an ATOH1-S328 non-phosphorylated form) was stable, whereas ATOH1-S328D (Ser 328 of ATOH1 was replaced with Asp; an ATOH1-S328 phosphomimic form) was fragile (Figure5—figure supplement 1D, F). However, the stability of ATOH1-S328D increased in the presence of MEIS1-FL or MEIS1-HdL (Figure5—figure supplement 1E, F), suggesting that both isoforms of MEIS1 inhibit ATOH1-degradation induced by phosphorylation at S328 of ATOH1. Next, GST-ATOH1 or GST-ATOH1-S328A and HA-Ub were co-transfected into N2a cells; pull-down and immunoblotting were subsequently performed with the indicated antibodies (Figure5—figure supplement 1G). The ubiquitination efficiency of S328A was lower than that of the wild-type (Figure5—figure supplement 1G upper panel), which is consistent with the observation that ATOH1-S328A is stable (Figure5—figure supplement 1D). Furthermore, the interaction of GST-ATOH1-S328A to CUL3 was much weaker than that of GST-ATOH1 to CUL3 (Figure5—figure supplement 1G second panel from the top), suggesting that binding of ATOH1 by CUL3 was facilitated by S328 phosphorylation.

S328 of ATOH1 is highly conserved among animal species and is predicted to be phosphorylated by protein kinases, including mitogen activated protein (MAP) kinases(Mulvaney and Dabdoub, 2012). To identify the MAP kinases responsible for S328 phosphorylation, N2a cells were transfected with GST-ATOH1 and then treated with MG132 and one of the indicated MAP kinase inhibitors, followed by pull-down with GST and immunoblotting with an ATOH1 or ATOH1 p-S328 antibody (Figure5—figure supplement 2A). The results showed that ATOH1- S328 phosphorylation was strongly inhibited by SCH772984 (an inhibitor of ERK), but not by c-Jun N-terminal kinase inhibitor IX or SB203580 (an inhibitor of p38), suggesting that ERK is involved in S328 phosphorylation. Next, we performed an *in vitro* kinase assay using recombinant ATOH1

253 and ERK1 proteins, followed by immunoblotting with an anti- ATOH1 p-S328 antibody. The result
254 clearly showed that ERK1 can directly phosphorylate ATOH1-S328 (Figure5—figure supplement
255 2B).
256 ERK signaling can be activated by BMPs(Cai et al., 2012), and BMP signaling is involved in
257 the degradation of ATOH1 in GCPs. In cultured GCPs, we found that ATOH1-S328 phosphorylation
258 was increased by BMP administration (Figure5—figure supplement 2C), suggesting that S328
259 phosphorylation by ERK is enhanced by BMP signaling in GCPs. Next, cultured GCPs were
260 incubated with BMP and MLN4924 (inhibitor of Cullin family proteins) or MG132, followed by
261 immunoblotting with ATOH1. Although BMP administration decreased ATOH1 protein, as expected,
262 the effect of BMP on ATOH1 levels was suppressed by coadministration of either MLN4924 or
263 MG132 (Figure5—figure supplement 2D, E). This result suggests that BMP-dependent degradation
264 of ATOH1 is elicited by CUL3 in GCPs. These findings suggest that the BMP-ERK signaling
265 phosphorylates ATOH1-S328, leading to ATOH1 degradation elicited by CUL3 in GCPs in the
266 developing cerebellum.
267
268 **MEIS1 inactivates CUL3 by promoting COP9 signalosome (CSN) and CUL3 complex binding**
269 We next investigated MEIS1-binding molecules in N2a cells. GST-tagged MEIS1-FL
270 (GST-MEIS1-FL) was transfected into N2a cells, precipitated using glutathione beads, and subjected
271 to LC–MS/MS (Figure6—figure supplement 1A), producing 1417 MEIS1-binding molecule
272 candidates (see Supplementary File). Interestingly, these included COPS2, COPS3, COPS4, COPS6,
273 COPS7a, and COPS8, CSN complex components (Figure 6A), suggesting that MEIS1 interacts with
274 the CSN complex. The CSN complex consists of eight components and suppresses substrate
275 polyubiquitination by Cullin family proteins. By competitively binding Cullin proteins, it masks
276 their substrate-binding regions, thus inhibiting their interactions with substrates(Chung and Dellaire,
277 2015). The CSN complex also suppresses neddylation, thereby suppressing Cullin protein function.
278 To confirm the interaction between the CSN complex and MEIS1, we transfected
279 GST-MEIS1-FL or GST-MEIS1-HdL into N2a cells, followed by pull-down with GST.
280 Immunoblotting with COPS2 showed that GST-MEIS1-FL or GST-MEIS1-HdL interacted with
281 endogenously expressed COPS2 (Figure 6B). Immunoblotting followed by LC–MS/MS did not
282 reveal the presence of COPS5, a known component of the CSN complex, indicating that both MEIS1
283 isoforms interacted with endogenous COPS5 (Figure 6B) and suggesting that MEIS1 interacts with
284 the CSN complex in cells.
285 We conducted similar pull-down and immunoblotting with HA-tagged COPS6 (HA-COPS6)
286 and GST-MEIS1-truncated mutant (1–130 aa) or GST-MEIS1 isoforms. As expected, HA-COPS6
287 was found to bind GST-MEIS1-FL and GST-MEIS1-HdL, whereas GST-MEIS1-1–130 did not bind
288 HA-COPS6 (Figure6—figure supplement 1B), consistent with the finding that MEIS1-1–130 does

not have ATOH1-stabilizing ability (Figure 4A).

Next, HA-COPS6 and GST-MEIS1-FL were transfected into N2a cells, followed by immunoprecipitation with HA and successive pull-down with GST. Immunoblotting revealed a significant signal for endogenous CUL3 (Figure 6C), suggesting that the CSN complex, MEIS1, and CUL3 form a tripartite complex in cells. Since the introduction of sh-*Cul3* did not affect the binding between HA-COPS6 and MEIS1-FL or MEIS1-HdL in N2a cells (Figure6—figure supplement 1C), we suggest that the interaction between the CSN complex and MEIS1 is not mediated by CUL3.

We then subjected lysates of GCPs purified from the P7 cerebellum to immunoprecipitation with the COPS5 antibody and immunoblotting with the MEIS1 antibody. We observed strong signals for MEIS1, suggesting that endogenous MEIS1 and the CSN complex interact with each other in cerebellar GCPs (Figure 6D). This MEIS1 signal was observed only for MEIS1-FL and not for MEIS1-HdL. However, this might be due to the very low expression of MEIS1-HdL in GCPs (Figure 1B, C). Given that MEIS1-HdL interacts with components of the CSN complex in N2a cells (Figure 6B, Figure6—figure supplement 1B, C), we believe that MEIS1-HdL may also interact with the CSN complex in GCPs.

To test the effect of MEIS1 expression on the interaction between CUL3 and the CSN complex, we transfected HA-COPS6 and MEIS1-FL or MEIS1-HdL into N2a cells and then performed immunoprecipitation with HA and immunoblotting. CUL3 interacted with HA-COPS6 (Figure 6E, lane 1), consistent with prior findings that cullin family proteins interact with the CSN complex(Chung and Dellaire, 2015). Further, CUL3 signals were significantly greater following co-transfection with MEIS1-FL or MEIS1-HdL (lane 2, 3, Figure 6F), suggesting that both MEIS1-FL and MEIS1-HdL enhance the CSN complex–CUL3 interaction.

Next, we transfected GST-ATOH1 and HA-Ub into N2a cells and then performed GST pull-down and immunoblotting with HA. As in the MG132 treatment, MEIS1-FL introduction reduced ATOH1 polyubiquitination, even in the absence of MG132 (Figure 6G, lane 1, 2). However, co-introduction of the knockdown vector for *Cops6* (sh-*Cops6*, Figure6—figure supplement 1D) ameliorated the effects of MEIS1-FL (Figure 6G, lane 3). These findings suggest that MEIS1 suppresses ATOH1 polyubiquitination and degradation by promoting the CSN complex–CUL3 interaction and by inhibiting the CUL3–ATOH1 interaction.

Given that MEIS1 inhibits CUL3 function by enhancing the CSN complex–CUL3 interaction, we proposed that MEIS1 may suppress the degradation of not only ATOH1 but also other CUL3-target proteins, such as NRF2(Jaramillo and Zhang, 2013), NCOA3(Ferry et al., 2011), and PP2A/C(Xu et al., 2014). When transfected into N2a cells, the expression of NRF2, NCOA3, and PP2A/C was much higher in the presence of MG132 (Figure6—figure supplement 1E, lane 4) than in the control (lane 1), consistent with previous findings that these proteins are degraded by CUL3-dependent polyubiquitination. Co-introduction of MEIS1-FL or MEIS1-HdL strongly

increased NRF2 and PP2A/C expression and moderately increased that of NCOA3 (lane 2, 3), relative to the control (lane 1), implying that MEIS1 isoforms broadly suppress CUL3-dependent protein degradation.

Transfected tagged COPS6 was expressed in both intracellular regions in N2a cells (Figure6—figure supplement 1F, consistent with a previous report that the CSN complex localizes in both the cell nucleus and cytoplasm. Essentially, similar COPS6 localization patterns were observed following co-transfection with MEIS1-FL or MEIS1-HdL (Figure6—figure supplement 1G, H), suggesting that neither MEIS1-FL nor MEIS1-HdL affect CSN-complex subcellular localization.

We then analyzed the ability of the two MEIS1 isoforms to suppress ATOH1 degradation. GST-ATOH1 was co-transfected with MEIS1-FL or MEIS1-HdL, using the indicated quantities of DNA (0–5 μg, Figure 6H). In contrast to MEIS1-FL, of which large amounts were required to suppress ATOH1 degradation, this was achieved using very little MEIS1-HdL (Figure 6H, I), suggesting that MEIS1-HdL suppresses ATOH1 degradation more effectively than MEIS1-FL. Fractionation using N2a cells transfected with ATOH1 and HA-Ub revealed that polyubiquitinated ATOH1 was localized in both the cytoplasm and nucleus (Figure 6J). In contrast, CUL3 was localized abundantly in the cytoplasm and negligibly in the nuclei (Figure 6J), consistent with prior suggestions(Anderica-Romero et al., 2013). These findings suggest that ATOH1 is polyubiquitinated by CUL3 in the cytoplasm, probably just after ATOH1 protein synthesis, while ATOH1 polyubiquitination in nuclei is elicited by other E3 ligases. MEIS1-HdL was localized exclusively in the cytoplasm, whereas MEIS1-FL was localized predominantly in the nucleus (Figure 1F–G), possibly accounting for their differential efficacy in suppressing CUL-3 dependent ATOH1 degradation.

The MEIS1–CSN pathway maintains GCPs in an immature state

Our in vitro experiments revealed that ATOH1 stabilization by MEIS1 was mediated by the CSN complex (Figure 6, Figure6—figure supplement 1). Further, MEIS1-HdL introduction into the EGL suppressed the differentiation from GCPs to GCs: 3 d after electroporation, the proportions of $Ki67^+$ and $ATOH1^+$ GCPs were higher, while those of $p27^+$ GCs were lower (Figure 2C–F).

To assess the involvement of the CSN complex in this MEIS1-HdL function, we introduced sh-*Cops6* with MEIS1-HdL into the EGL, under the experimental conditions shown in Figure 2C. The effects of MEIS1-HdL were rescued by cointroduction with sh-*Cops6* to the same extent as sh-*Meis1*-HdL single introduction (Figure 7A–E). This suggests that COPS9 is required for MEIS1-HdL to function in GCPs, and that the CSN complex works with MEIS1-HdL to suppress the GCP differentiation into GCs, during cerebellar development(Figure 7F).

Discussion

Cullin family proteins, including CUL3, are known to be inactivated by the COP9 signalosome(Chung and Dellaire, 2015). The COP9 signalosome inhibits the binding of Cullin to its target proteins by deneddylation of Cullin family proteins or by binding directly to Cullin family proteins. Inositol hexakisphosphate reduces the functions of E3-ligase by enhancing the binding of CUL1 and CUL4A to the COP9 signalosome(Scherer et al., 2016). We found that MEIS1 promotes the binding of CUL3 to the COP9 signalosome in a transcription-independent manner.

The stabilization efficiency of ATOH1 is higher in MEIS1-HdL than in MEIS1-FL. This is likely because CUL3 and MEIS1-HdL are localized in the cytoplasm, making it easier for these proteins to form a complex. Our proteomic analysis showed that CUL1 and CUL4 may also bind to MEIS1, suggesting that MEIS1 is involved in the inactivation of not only CUL3 but also other Cullin family proteins. If this is the case, the localization of Cullin family proteins to the cell nuclei, such as CUL1 and CUL4B, may be inactivated by MEIS1-FL, which localizes preferentially to the nuclei.

It has been reported that the phosphorylation of ATOH1 is largely related to the stability of ATOH1 protein. In studies of human ATOH1 protein, phosphorylation at S54 and S58 (corresponding to S52 and S56 in mice, respectively) was shown to reduce the protein stability(Tsuchiya et al., 2007). In mouse ATOH1, phosphorylation at S328, S331, S334, and S339 and that at Y78 and S309 reduces and enhances the stability of ATOH1, respectively(Cheng et al., 2016; Forget et al., 2014; Klisch et al., 2017; Miyashita et al., 2021). To date, glycogen synthase kinase 3β(Tsuchiya et al., 2007), casein kinase 1δ(Cheng et al., 2016), Janus kinase 2(Klisch et al., 2017), and several cyclin-dependent kinases(Miyashita et al., 2021; Tomic et al., 2018) have been reported to phosphorylate ATOH1. We identified a novel kinase for ATOH1, ERK, which is involved in BMP signaling-dependent phosphorylation and degradation of ATOH.

COPS5 and COPS6, which are known components of the COP9 signalosome, are highly expressed in a variety of human cancers(Lee et al., 2011). In transgenic mice overexpressing *Cops5*, the pool of hematopoietic stem cells increased, and symptoms of myeloproliferative diseases were observed(Mori et al., 2008). This phenotype is partly similar to the phenotype of Meis1 overexpression in hematopoietic stem cells(Lawrence et al., 1999). Considering the coordinated function of MEIS1 and COP9 signalosome in GCPs, MEIS1 and the COP9 signalosome may also be involved in myeloproliferative diseases. To date, the involvement of MEIS1 in several tumors and myeloproliferative diseases was thought to be related to the transcriptional regulatory ability of MEIS1. However, occurrence of some of the tumors or diseases may not be directly associated with the transcriptional regulatory capacity of MEIS1. The targets of Cullin family proteins include molecules that contribute to cancer onset or growth, such as NRF2 and ATOH1. Suppression of Cullin family proteins by the MEIS1 and COP9 signalosome may limit the degradation of key proteins and exacerbate cancer.

MYC-nick is a functional molecule that, like MEIS1-HdL, has lost its DNA-binding domain. MYC-nick is a protein fragment produced from c-MYC by calpain cleavage to remove the nuclear localization sequence and DNA-binding domain. Although c-MYC is localized in the nucleus, MYC-nick, like MEIS1-HdL, is found in the cytoplasm. Whereas c-MYC acts in the nucleus to regulate the transcription of various genes, MYC-nick recruits the histone acetyltransferase GCN5 to microtubules in the cytoplasm and promotes the acetylation of α-tubulin(Conacci-Sorrell et al., 2010).

In animals, the levels of important proteins are strictly regulated. The proteolytic regulatory system is widely involved in the development, function, and pathology of the nervous system. We found that ATOH1, the protein responsible for the undifferentiated and proliferative properties of GCPs, is tightly regulated by extracellular signals, kinases, E3-ligases, and ubiquitination inhibitory molecules such as MEIS1 and the COP9 signalosome. These properties have important implications for understanding the regulation of neural progenitor cell to neuron differentiation.

Materials and methods

Animals

All animal experiments in this study were approved by the Animal Care and Use Committee of the National Institute of Neuroscience, National Center of Neurology and Psychiatry (Tokyo, Japan; project 2019028R2). Mice were housed in SPF with food and water ad libitum. ICR pups were obtained from SLC (Japan). Atoh1^{AtGFP} (The Jackson Laboratory: B6.129S-*Atoh1*$^{tm4.1Hzo}$/J, Stock No: 013593) and Ki67^{KiRFP} (The Jackson Laboratory: *Mki67*$^{tm1.1Cle}$/J, Stock No: 029802) mice were obtained from The Jackson Laboratory. For immunohistochemistry, neonatal mice were fixed with 4% PFA and embedded sagittally with ProLong™ Glass Antifade Mountant (Thermo Fisher Scientific P36980). Frozen brains were sectioned into thin slices via cryostat (Leica Biosystems).

Quantitative PCR (qPCR)

GCP isolation and qPCR was performed as previously described(Adachi et al., 2021). Isolated GCPs were suspended in cold DPBS containing 1% BSA. Cell sorting was performed in FACSAriaTM Fusion. Gating of GFP and RFP negative populations was performed using GCPs from WT mice. Fluorescence compensation of RFP and GFP was performed using GCP of Ki67$^{KiRFP/+}$ or Atoh1$^{AtGFP/+}$ mice. Cells were sorted into cold DPBS containing 1% BSA and centrifuged at 800 × *g* for 3 min.

cDNA was generated with Superscript IIkit (Invitrogen). Relative gene expression was compared with the geometric mean of *18s rRNA*. The primer sequences used are as following:
18s rRNA: CCCGAAGCGTTTACTTTGAA and CCCTCTTAATCATGGCCTCA,

Meis1-FL: ACAGCAGTGAGCAAGGTG and CAGAAGGGTAAGGGTGTGTT,
Meis1-HdL: TGAGCAAGCACCCTTACCCTTCTGAA and GACTGCTCGGTTGGACTG,
Atoh1: AGCTTCCTCTGGGGGTTACT and TTCTGTGCCATCATCGCTGT.

Plasmids

The expression vectors of Atoh1, Meis1 1-130aa and Meis1-FL were cloned from cDNAs from C57/BL6 mouse cerebellum. Cloned fragments were inserted into a pCAGGS vector or pEF-BOS-GST vectors (gifts from K. Kaibuchi, Fujita Health University, Nagoya, Japan) vector and cloned sequences confirmed by sequencing. pCAG-H3.1-EGFP vector was a gift from Dr. N. Masuyama. HA-Ub vector was kindly provided by Dr. S. Wakatsuki (NCNP, Tokyo, Japan). Flag-HA-Cops6 was purchased from addgene (Plasmid #22542). Meis1-HdL, Res-Meis1-HdL and mutated forms of Atoh1 S328A and S328D were generated following the mutagenesis protocol of PrimeStarMax (Takara). The primers we used to create Res-Meis1-HdL were GAGCAGGCCCCTTTACCCTTCTGAAGAACA and TAAAGGGGCCTGCTCACTGCTGTTATCCCC. shRNAs were generated by inserting the double-stranded oligonucleotides into a mU6 pro vector. The targeting sequence of each shRNAs was designed by siDirect 2.0(Naito et al., 2009) and the target sequences are indicated below.
sh-Meis1-HdL: 5′- CAGTGAGCAAGCACCCTTA-3′,
sh-Meis1-all: 5′- GCACAAGATACAGGACTTACC -3′(Owa et al., 2018),
sh-Cul3: 5′- GAAAGAAACAAGACAGAAAG -3′,
sh-Cops6-1: 5′-ACCAAGGAGGAGCAGTTTAAA -3′,
sh-Cops6-2: 5′-TTGAGTCTGTCATCGATATAA -3′.

Cell culture, transfection, and drug treatment

N2a cells were obtained from ATCC (Manassas, VA, USA) and cultured in Dulbecco's modified Eagle medium (DMEM) containing 10% fetal bovine serum (FBS) and 100 U/ml penicillin–streptomycin. Transfection of N2a cells was performed using transfection reagent (Bio-Rad, Hercules, CA, USA).

Five million P7 GCPs were plated per well in a six-well plate and cultured for 48 h in the presence of 200 nM smoothened agonist.

Cycloheximide (100 μM) was diluted in dimethyl sulfoxide (DMSO) and added to N2a cells, as indicated. BMP4 (100 ng/ml) diluted in Milli-Q water, 500 nM MLN4924, 10 μM SCH772984, 25 μM JNK inhibitor IX, 10 μM SB203580 and 10 μM MG132 diluted in DMSO were administered to the cultured cells indicated, after which cells were harvested at the indicated times.

Immunohistochemistry

469 Tissues were fixed with 4% paraformaldehyde (PFA) in PBS and cryoprotected with 30% sucrose
470 in PBS. After tissues were embedded in optimal cutting temperature (OCT) compound, cryosections
471 were made at 16 μm. Sections were incubated in blocking buffer containing 1% BSA and 0.1%
472 Triton X-100 in PBS at room temperature (RT) for 1 h and subsequently immunolabeled using the
473 following primary antibodies in blocking buffer at 4 °C overnight. Specimens were subsequently
474 rinsed with PBS and incubated with secondary antibodies conjugated with Alexa Fluor 488, Alexa
475 Fluor 568, Alexa Fluor 594, or Alexa Fluor 647 (1:400; Invitrogen) and DAPI (1:3,000; Invitrogen)
476 in blocking buffer containing 1% BSA and 0.2% Triton X-100 in PBS at RT for 2 h. Fluorescence
477 images were acquired using a Zeiss LSM 780 confocal microscope system (Carl Zeiss) and ZEN
478 2009 software. Quantification of the fluorescence intensity of immunolabeled cells was performed
479 using the "Measure" functions of ImageJ. Antibodies used in this study were as follows:
480 anti-ATOH1 antibody (homemade, rabbit), anti-KI67 antibody (eBioscience, 14-5698-82, rat),
481 anti-p27 antibody (MBL, 554, rabbit), anti-HA(C29F4) (CST, 3724S, rabbit), anti-GFP antibody
482 (kind gift from Dr. A. Imura, Foundation for Biomedical Research and Innovation, Kobe, Japan rat),
483 anti-GFP (Aves Labs, GFP-1010, chicken).
484
485 ***In vivo* electroporation**
486 In vivo electroporation in neonatal mice has been described previously (Owa et al, 2018).
487 Expression plasmids were diluted to 1 μg/μl, shRNAs to 2 μg/μl, and pCAG-H2BGFP to 0.5 μg/μl in
488 Milli-Q water (Millipore). Fast Green was added to visualize the plasmid solutions, which were
489 injected into P8 ICR cerebella over the skull. Mice received electric pulses (80 V for 50 ms, with
490 150 ms intervals) using forceps-type electrodes (NEPA Gene, Chiba, Japan). The pups were kept
491 warm at 37 °C during recuperation and returned to the litter after fully recovering. Pups were fixed
492 with 4% PFA for 3 days after electroporation.
493
494 **Immunoblotting**
495 Detailed protocols have been described previously(Shiraishi et al., 2019). Briefly, proteins were
496 transferred to polyvinylidene fluoride membranes, which were incubated with primary antibodies at
497 4 °C overnight. After the membranes were incubated with secondary antibodies at room temperature
498 for 2 h, horseradish peroxidase substrate (Millipore) was applied, and immuno-signals were detected
499 using a LAS4000 system (Fujifilm) and FUSION SOLO S (Vilber). Antibodies used in this study
500 were as follows: anti-GAPDH (CST, #2118, rabbit), anti-GST (CST, #2622, rabbit), anti-HA (CST,
501 #3724, rabbit), anti- ATOH1 (homemade, rabbit), anti-Meis1 (abcam, ab19867, rabbit), anti-CUL3
502 (CST, #2759, rabbit), anti-COPS2 (Bethyl Laboratories, A300-028A, rabbit), anti-COPS5 (Bethyl
503 Laboratories, A300-014A, rabbit), anti-SRC-3 (NCOA3; CST, #2126, rabbit), anti-PP2A/C subunit
504 (CST, #2038, rabbit), anti-NRF2 (Novusbio, NBP1-32822, rabbit), anti-LAMIN A/C (CST, #4777,

505 mouse), anti-βIIITUBULIN (Millipore, MAB1637, mouse), and anti-ATOH1 p-S328 (homemade,
506 rabbit).
507
508 **GST pull-down assay, protein purification, and phospho-MS**
509 GST-tagged vectors expressing Atoh1, Atoh1 (S328A), Atoh1(S328D), Meis1-FL, and Meis1-HdL
510 were transfected into N2a cells, which were cultured for 2 days. Cells were harvested, as described,
511 and after lysis, supernatants were incubated with glutathione-conjugated Sepharose beads (GE
512 healthcare) at 4 °C overnight. Sepharose beads were washed twice and resuspended in sample buffer.
513 For protein purification, washed sepharose beads were incubated with TED buffer containing 150
514 mg of reduced-form glutathione (pH 7.4) at 4 °C for 30 min, and the supernatants were stored at
515 -80 °C. Phospho-MS was performed, as previously described (Nagai et al, 2016).
516
517 **In vitro kinase assay**
518 Purified ATOH1 (5 μg) was incubated with TED buffer containing 20 μM ATP, 0.5 μCi
519 [k-32P]-ATP, 20 mM $MgCl_2$, and between 3 and 5 μg of ERK1 (SCP, M29-10U) at 37 °C for 1 h.
520 The reacted solution was then applied to the sample buffer and subjected to SDS–polyacrylamide gel
521 electrophoresis. Phosphorylation signals were detected using a Typhoon system (GE Healthcare).
522
523 **Statistical analyses**
524 Pairwise comparisons between the means of different groups were performed using a Student's *t*
525 test (two tailed, unpaired). The difference between two subsets of data was considered statistically
526 significant if the Student's *t* test gave a significance level of $*p < 0.05$, $**p < 0.01$, or $***p < 0.001$.
527 The data are reported as the mean ± SEM.
528
529 **Acknowledgements**
530 This work was supported by Grants-in-Aid for Scientific Research, KAKENHI
531 (Grant 16H06528 and 18H02538 for M.H.); AMED (19dm0107085h0004; JP21wm0425005 to
532 M.H.), an Intramural Research Grant of NCNP (Grants 30-9 and 1-4 for M.H.), Japan Health
533 Research Promotion Bureau (JH) under Research Fund (Grant 2020-B-07 for M.H).
534
535 **Competing interests**
536 The authors declare that they have no conflict of interest.
537
538 **References**
539
540 **Adachi, T., Miyashita, S., Yamashita, M., Shimoda, M., Okonechnikov, K., Chavez, L., Kool, M., Pfister,**

541 S.M., Inoue, T., Kawauchi, D., *et al.* (2021). Notch Signaling between Cerebellar Granule Cell
542 Progenitors. eNeuro *8*.
543 Anderica-Romero, A.C., Gonzalez-Herrera, I.G., Santamaria, A., and Pedraza-Chaverri, J. (2013).
544 Cullin 3 as a novel target in diverse pathologies. Redox Biol *1*, 366-372.
545 Ayrault, O., Zhao, H., Zindy, F., Qu, C., Sherr, C.J., and Roussel, M.F. (2010). Atoh1 inhibits neuronal
546 differentiation and collaborates with Gli1 to generate medulloblastoma-initiating cells. Cancer Res
547 *70*, 5618-5627.
548 Azcoitia, V., Aracil, M., Martinez, A.C., and Torres, M. (2005). The homeodomain protein Meis1 is
549 essential for definitive hematopoiesis and vascular patterning in the mouse embryo. Dev Biol *280*,
550 307-320.
551 Baek, K., Scott, D.C., and Schulman, B.A. (2021). NEDD8 and ubiquitin ligation by cullin-RING E3
552 ligases. Curr Opin Struct Biol *67*, 101-109.
553 Cai, J., Pardali, E., Sanchez-Duffhues, G., and ten Dijke, P. (2012). BMP signaling in vascular diseases.
554 FEBS Lett *586*, 1993-2002.
555 Cheng, Y.F., Tong, M., and Edge, A.S. (2016). Destabilization of Atoh1 by E3 Ubiquitin Ligase Huwe1
556 and Casein Kinase 1 Is Essential for Normal Sensory Hair Cell Development. J Biol Chem *291*,
557 21096-21109.
558 Chua, Y.S., Boh, B.K., Ponyeam, W., and Hagen, T. (2011). Regulation of cullin RING E3 ubiquitin
559 ligases by CAND1 in vivo. PLoS One *6*, e16071.
560 Chung, D., and Dellaire, G. (2015). The Role of the COP9 Signalosome and Neddylation in DNA
561 Damage Signaling and Repair. Biomolecules *5*, 2388-2416.
562 Conacci-Sorrell, M., Ngouenet, C., and Eisenman, R.N. (2010). Myc-nick: a cytoplasmic cleavage
563 product of Myc that promotes alpha-tubulin acetylation and cell differentiation. Cell *142*, 480-493.
564 Crist, R.C., Roth, J.J., Waldman, S.A., and Buchberg, A.M. (2011). A conserved tissue-specific
565 homeodomain-less isoform of MEIS1 is downregulated in colorectal cancer. PLoS One *6*, e23665.
566 Ferry, C., Gaouar, S., Fischer, B., Boeglin, M., Paul, N., Samarut, E., Piskunov, A., Pankotai-Bodo, G.,
567 Brino, L., and Rochette-Egly, C. (2011). Cullin 3 mediates SRC-3 ubiquitination and degradation to
568 control the retinoic acid response. Proc Natl Acad Sci U S A *108*, 20603-20608.
569 Flora, A., Klisch, T.J., Schuster, G., and Zoghbi, H.Y. (2009). Deletion of Atoh1 disrupts Sonic
570 Hedgehog signaling in the developing cerebellum and prevents medulloblastoma. Science *326*,
571 1424-1427.
572 Forget, A., Bihannic, L., Cigna, S.M., Lefevre, C., Remke, M., Barnat, M., Dodier, S., Shirvani, H.,
573 Mercier, A., Mensah, A., *et al.* (2014). Shh signaling protects Atoh1 from degradation mediated by
574 the E3 ubiquitin ligase Huwe1 in neural precursors. Dev Cell *29*, 649-661.
575 Geerts, D., Schilderink, N., Jorritsma, G., and Versteeg, R. (2003). The role of the MEIS homeobox
576 genes in neuroblastoma. Cancer Lett *197*, 87-92.

577 Heine, P., Dohle, E., Bumsted-O'Brien, K., Engelkamp, D., and Schulte, D. (2008). Evidence for an
578 evolutionary conserved role of homothorax/Meis1/2 during vertebrate retina development.
579 Development *135*, 805-811.
580 Helms, A.W., Gowan, K., Abney, A., Savage, T., and Johnson, J.E. (2001). Overexpression of MATH1
581 disrupts the coordination of neural differentiation in cerebellum development. Mol Cell Neurosci
582 *17*, 671-682.
583 Hisa, T., Spence, S.E., Rachel, R.A., Fujita, M., Nakamura, T., Ward, J.M., Devor-Henneman, D.E., Saiki,
584 Y., Kutsuna, H., Tessarollo, L., *et al.* (2004). Hematopoietic, angiogenic and eye defects in Meis1
585 mutant animals. EMBO J *23*, 450-459.
586 Imamura, T., Morimoto, A., Takanashi, M., Hibi, S., Sugimoto, T., Ishii, E., and Imashuku, S. (2002).
587 Frequent co-expression of HoxA9 and Meis1 genes in infant acute lymphoblastic leukaemia with
588 MLL rearrangement. Br J Haematol *119*, 119-121.
589 Jaramillo, M.C., and Zhang, D.D. (2013). The emerging role of the Nrf2-Keap1 signaling pathway in
590 cancer. Genes Dev *27*, 2179-2191.
591 Klisch, T.J., Vainshtein, A., Patel, A.J., and Zoghbi, H.Y. (2017). Jak2-mediated phosphorylation of
592 Atoh1 is critical for medulloblastoma growth. Elife *6*.
593 Komuro, H., and Yacubova, E. (2003). Recent advances in cerebellar granule cell migration. Cell Mol
594 Life Sci *60*, 1084-1098.
595 Lawrence, H.J., Rozenfeld, S., Cruz, C., Matsukuma, K., Kwong, A., Komuves, L., Buchberg, A.M., and
596 Largman, C. (1999). Frequent co-expression of the HOXA9 and MEIS1 homeobox genes in human
597 myeloid leukemias. Leukemia *13*, 1993-1999.
598 Lee, M.H., Zhao, R., Phan, L., and Yeung, S.C. (2011). Roles of COP9 signalosome in cancer. Cell Cycle
599 *10*, 3057-3066.
600 Miyashita, S., Owa, T., Seto, Y., Yamashita, M., Aida, S., Sone, M., Ichijo, K., Nishioka, T., Kaibuchi, K.,
601 Kawaguchi, Y., *et al.* (2021). Cyclin D1 controls development of cerebellar granule cell progenitors
602 through phosphorylation and stabilization of ATOH1. EMBO J, e105712.
603 Mori, M., Yoneda-Kato, N., Yoshida, A., and Kato, J.Y. (2008). Stable form of JAB1 enhances
604 proliferation and maintenance of hematopoietic progenitors. J Biol Chem *283*, 29011-29021.
605 Mulvaney, J., and Dabdoub, A. (2012). Atoh1, an essential transcription factor in neurogenesis and
606 intestinal and inner ear development: function, regulation, and context dependency. J Assoc Res
607 Otolaryngol *13*, 281-293.
608 Naito, Y., Yoshimura, J., Morishita, S., and Ui-Tei, K. (2009). siDirect 2.0: updated software for
609 designing functional siRNA with reduced seed-dependent off-target effect. BMC Bioinformatics *10*,
610 392.
611 Owa, T., Taya, S., Miyashita, S., Yamashita, M., Adachi, T., Yamada, K., Yokoyama, M., Aida, S., Nishioka,
612 T., Inoue, Y.U., *et al.* (2018). Meis1 Coordinates Cerebellar Granule Cell Development by Regulating

613 Pax6 Transcription, BMP Signaling and Atoh1 Degradation. J Neurosci *38*, 1277-1294.
614 Petroski, M.D., and Deshaies, R.J. (2005). Function and regulation of cullin-RING ubiquitin ligases.
615 Nat Rev Mol Cell Biol *6*, 9-20.
616 Scherer, P.C., Ding, Y., Liu, Z., Xu, J., Mao, H., Barrow, J.C., Wei, N., Zheng, N., Snyder, S.H., and Rao,
617 F. (2016). Inositol hexakisphosphate (IP6) generated by IP5K mediates cullin-COP9 signalosome
618 interactions and CRL function. Proc Natl Acad Sci U S A *113*, 3503-3508.
619 Schulte, D., and Geerts, D. (2019). MEIS transcription factors in development and disease.
620 Development *146*.
621 Shiraishi, R.D., Miyashita, S., Yamashita, M., Adachi, T., Shimoda, M.M., Owa, T., and Hoshino, M.
622 (2019). Expression of transcription factors and signaling molecules in the cerebellar granule cell
623 development. Gene Expr Patterns *34*, 119068.
624 Spieker, N., van Sluis, P., Beitsma, M., Boon, K., van Schaik, B.D., van Kampen, A.H., Caron, H., and
625 Versteeg, R. (2001). The MEIS1 oncogene is highly expressed in neuroblastoma and amplified in
626 cell line IMR32. Genomics *71*, 214-221.
627 Tomic, G., Morrissey, E., Kozar, S., Ben-Moshe, S., Hoyle, A., Azzarelli, R., Kemp, R., Chilamakuri,
628 C.S.R., Itzkovitz, S., Philpott, A., *et al.* (2018). Phospho-regulation of ATOH1 Is Required for
629 Plasticity of Secretory Progenitors and Tissue Regeneration. Cell Stem Cell *23*, 436-443 e437.
630 Tsuchiya, K., Nakamura, T., Okamoto, R., Kanai, T., and Watanabe, M. (2007). Reciprocal targeting of
631 Hath1 and beta-catenin by Wnt glycogen synthase kinase 3beta in human colon cancer.
632 Gastroenterology *132*, 208-220.
633 Tucker, E.S., Lehtinen, M.K., Maynard, T., Zirlinger, M., Dulac, C., Rawson, N., Pevny, L., and Lamantia,
634 A.S. (2010). Proliferative and transcriptional identity of distinct classes of neural precursors in
635 the mammalian olfactory epithelium. Development *137*, 2471-2481.
636 Wu, C., Macleod, I., and Su, A.I. (2013). BioGPS and MyGene.info: organizing online, gene-centric
637 information. Nucleic Acids Res *41*, D561-565.
638 Xu, J., Zhou, J.Y., Xu, Z., Kho, D.H., Zhuang, Z., Raz, A., and Wu, G.S. (2014). The role of
639 Cullin3-mediated ubiquitination of the catalytic subunit of PP2A in TRAIL signaling. Cell Cycle *13*,
640 3750-3758.
641 Zhao, H., Ayrault, O., Zindy, F., Kim, J.H., and Roussel, M.F. (2008). Post-transcriptional
642 down-regulation of Atoh1/Math1 by bone morphogenic proteins suppresses medulloblastoma
643 development. Genes Dev *22*, 722-727.
644
645

Figure Legends

Figure 1. Meis1 is strongly expressed in ATOH1-expressing GCPs and localizes in the cytoplasm.

A. Schematic of MEIS1-FL and MEIS1-HdL mRNA and protein.

B. Meis1 PCR amplification using a negative control (RT^{-}), plasmids coding for Meis1-FL or Meis1-HdL, or P6 GCP cDNA templates. Meis1-FL and Meis1-HdL were detected in GCP cDNA.

C. Immunoblotting with anti-MEIS1 antibody from P6 GCP cell lysate, after immunoprecipitation with an MEIS1 antibody. A large amount of MEIS1-FL and a small amount of MEIS1-HdL, were detected in the GCP lysate.

D. Schematic of GCP separation via FACS, using Atoh1-GFP/$^{+}$; Ki67-RFR/$^{+}$ mice.

E. *Meis1-FL* and *Meis1-HdL* expression was estimated via quantitative RT-PCR, using FACS-sorted GCP cells purified from P6 cerebella. We used Meis1-HdL- and Meis1-FL-specific primers.

F. N2a cells were fractionated into the cytoplasmic and nuclear fractions for western blotting. Equal amounts of protein were separated via SDS-PAGE and blotted for MEIS1, βIII-TUBULIN (the cytoplasmic fraction loading control), and LAMIN A/C (the nuclear fraction loading control). Arrowheads indicate MEIS1-FL, and arrows indicate MEIS1-HdL.

G and H. N2a cells transfected with Meis1-FL-EGFP (**G**) or Meis1-HdL-EGFP (**H**) and immunostained for GFP (green) and DAPI (blue). Scale bar, 10 μm.

Figure 2. MEIS1-HdL maintains the undifferentiated state of GCPs, while MEIS1-FL promotes GC differentiation.

A–F. Immunostaining with GFP (yellow), KI67 (cyan), and ATOH1 (magenta) in P11 cerebella electroporated with H3.1-EGFP only (**A**), Meis1-FL and H3.1-EGFP (**B**), or Meis1-HdL and H3.1-EGFP(**C**) at P8. Electroporated-cell nuclei were labeled with H3.1-EGFP (yellow).

Electroporated-cell differentiation was evaluated using the expression of KI67 (**D**), p27 (**E**), and ATOH1 (**F**). **a–c**: n = 4 mice

Figure 3. Endogenous Meis1-HdL participates in maintaining GCPs in an immature and proliferative state.

A–F. Immunostaining with GFP (yellow), KI67 (cyan), and ATOH1 (magenta) in P11 cerebellar cells electroporated with sh-*Meis1-HdL* and H3.1-EGFP (**A**), sh-*Meis1-HdL*, Res-Meis1-HdL, and H3.1-EGFP (**B**), or sh-*Meis1-all* and H3.1-EGFP (**C**) at P8. Electroporated-cell nuclei were labeled with H3.1-EGFP (yellow).

Electroporated-cell differentiation was evaluated using the expression of KI67 (**D**), p27 (**E**), and

ATOH1 (**F**). **a, b**: n = 4 mice; **c**: n = 3 mice.

Figure 4. MEIS1 stabilizes ATOH1 levels in a homeodomain-independent manner.

A. Immunoblotting analyses with the indicated antibodies (ATOH1, GAPDH) on lysates from N2a cells transfected with GST-Atoh1 and the indicated Meis1 plasmids. At 48 h after transfection, the cells were treated with or without MG132 for 6 h.

B. N2a cells transfected with GST-Atoh1 and Meis1-HdL or Meis1-FL plasmids were harvested after 0, 4, and 8 h of treatment with 50 μg/mL cycloheximide (Chx). The lysates were immunoblotted with anti-ATOH1 or GAPDH. Some of the cells were treated with MG132 at 6 h before Chx administration.

C. ATOH1 levels, relative to those of GAPDH in **B**.

Figure 5. MEIS1 inhibits CUL3 binding to ATOH1, suppressing ATOH1 ubiquitination and stabilizing ATOH1

A. N2a cells transfected with GST-Atoh1, HA-ubiquitin (HA-Ub), and Meis1-FL or Meis1-HdL were treated with MG132 for 6 h. After GST pull-down, ATOH1 ubiquitination (upper panel) and total ATOH1 levels (lower panel) were determined using immunoblotting with an anti-HA antibody and anti-GST antibody.

B. HA(Ub) levels, relative to those of GST in **A**.

C. Schematic of proteomic analysis to identify molecules binding to ATOH1 in the presence or absence of MEIS1.

D. Ubiquitin-related proteins that reduced binding to ATOH1 in the presence of MEIS1.

E. N2a cells were transfected with GST-Atoh1 alone or with GST-Atoh1, Meis1-FL, or Meis1-HdL. After GST pull-down, CUL3 interaction was determined by immunoblotting with an anti-CUL3 antibody. In the presence of MEIS1-FL or MEIS1-HdL, binding of ATOH1 and CUL3 was reduced.

F. N2a cells were transfected with GST-Atoh1, HA-Ub, sh-Scramble, or sh-*Cul3* plasmids. After GST pull-down, ATOH1 ubiquitination (upper panel) and total ATOH1 levels were determined using immunoblotting with an anti-HA antibody and anti-GST antibody. CUL3 expression was measured using immunoblotting the input sample with the CUL3 antibody (lower panel). The ubiquitin level of ATOH1 was reduced by *Cul3*-knockdown.

G. N2a cells transfected with GST-Atoh1 and sh-*Cul3* plasmids were harvested after 0, 4, and 8 h of treatment with 50 μg/mL Chx. The lysates were immunoblotted with anti-ATOH1 or GAPDH.

H. ATOH1 levels, relative to those of GAPDH in **G**.

Figure 6. MEIS1-FL and MEIS1-HdL promote CUL3 binding to the Cop9 signalosome complex and eventually inactivate CUL3

A. Components of the COP9 signalosome complex, identified by proteomic analysis of MEIS1 binding candidates. The experimental scheme is shown in Figure S7 A.

B. N2a cells were transfected with GST, GST-Meis1-FL, or Meis1-HdL. After GST pull-down, interactions of COPS2 and COPS5 with GST-tagged protein were determined using immunoblotting with an anti-COPS2 antibody, anti-COPS5 antibody, and anti-GST antibody.

C. N2a cells were transfected with Flag-HA-Cops6 and GST or GST-Mei1-FL. Following sequential immunoprecipitation with an anti-HA antibody and pull-down with GST, immunoblotting was performed with anti-CUL3 antibody. Tripartite CUL3–MEIS1–COPS6 binding was detected.

D. COPS5 was immunoprecipitated from P6 GCP cells. The resulting complexes were analyzed using immunoblotting with anti-COPS5 and anti-MEIS1 antibodies.

E. N2a cells were transfected with Flag-HA-Cops6 alone or in combination with Meis1-FL or Meis1-HdL. After immunoprecipitation with an anti-HA antibody, the interactions of CUL3 and MEIS1 with COPS6 were determined using immunoblotting with anti-CUL3, anti-MEIS1, and anti-HA antibodies. In the presence of MEIS1-FL or MEIS1-HdL, the binding efficiency of CUL3 and COPS6 was increased.

F. CUL3 signal intensity in **E**.

G. N2a cells were transfected with GST-Atoh1 and HA-Ub, or with GST-Atoh1, HA-Ub, or Meis1-FL and sh-scramble or sh-*Cops6*. After GST pull-down, ATOH1 ubiquitination (upper panel) and total ATOH1 levels (lower panel) were determined using immunoblotting with anti-HA and anti-GST antibodies. Inhibition of ATOH1 ubiquitination by MEIS1 was cancelled by *Cops6* knockdown.

H. Immunoblotting was performed using lysates of N2a cells transfected with GST-Atoh1 plasmid and the indicated amount of Meis1 plasmid, with the indicated antibodies for ATOH1, MEIS1, and GAPDH.

I. ATOH1 level as a percentage of the GAPDH level in **H**, against the concentration of the MEIS1 vector. The means ± SEMs (relative to 0 μg of the Meis1 plasmid), are based on three trials under each condition.

J. N2a cells transfected with Atoh1 and HA-Ub were fractionated into the cytoplasmic and nuclear fractions for western blotting. Equal amounts of protein were separated by SDS-PAGE and blotted for ATOH1, CUL3, βIII-TUBULIN (cytoplasmic fraction loading control), and LAMIN A/C (nuclear fraction loading control). ATOH1 ubiquitination was detected in both the cytoplasm and nucleus. CUL3 was strongly localized in the cytoplasmic fraction.

Figure 7. The COP9 signalosome is required for the maintenance of the undifferentiated state by Meis1-HdL in GCPs.

A. Immunostaining with GFP (yellow), KI67 (cyan), and ATOH1 (magenta) in P11 cerebella

electroporated with Meis1-HdL, H3.1-EGFP, and sh-*Cops6* at P8.

B. Immunostaining with GFP (green) and p27 (magenta) in P11 cerebella electroporated with Meis1-HdL, H3.1-EGFP, and sh-*Cops6* at P8.

C–E. Differentiation of electroporated cells was evaluated by measuring the expression of KI67 (**C**), p27 (**D**), and ATOH1 (**E**). n = 3 mice.

F. Schematic diagram of MEIS1-HdL function in GCP.

Supplemental Information Legends

Figure 1--figure supplement 1. Isolation of three types of GC-lineage cells using Atoh1$^{AtGFP/+}$; Ki67$^{KiRFP\ /+}$ mice.

A. Immunostaining with GFP (green) and ATOH1 (magenta) in the cerebella of P7 **Atoh1$^{AtGFP/+}$; Ki67$^{KiRFP\ /+}$** mice.

B. Immunostaining with KI67 (green) and RFP (magenta) in the cerebella of P7 **Atoh1$^{AtGFP/+}$; Ki67$^{KiRFP\ /+}$** mice.

C. Immunostaining with GFP (green) and RFP (magenta) in the cerebella of P7 **Atoh1$^{AtGFP/+}$; Ki67$^{KiRFP\ /+}$** mice.

D. FACS plots representing GFP^{-} and RFP^{+} cells from the purified GCPs of WT, **Atoh1$^{AtGFP/+}$; Ki67$^{KiRFP\ /+}$**; **Ki67$^{KiRFP\ /+}$** mice.

E. *Atoh1* expression estimated by qRT-PCR using FACS-sorted GCP cells purified from P6 cerebella. Scale bar, 10 μm.

Figure 2--figure supplement 1. Meis1-HdL overexpression reduces the number of p27^{+} cells, while Meis1-FL overexpression increases it.

A-C. Immunostaining with GFP (green), and p27 (magenta) in P11 cerebella electroporated with H3.1-EGFP alone (**A**), Meis1-FL and H3.1-EGFP (**B**), or Meis1-HdL and H3.1-EGFP (**C**) at P8. Electroporated-cell nuclei were labeled with H3.1-EGFP (green). Scale bar, 20 μm.

Figure 3--figure supplement 1. Meis1-HdL knockdown promotes GCP differentiation.

A. Left panel: N2a cells were transfected with Meis1-FL, Meis1-HdL, sh-Scramble, or sh-*Meis1-HdL* plasmid, and the protein levels were checked by western blotting with the MEIS1 antibody. The sh-*Meis1-HdL* plasmid knocks down only *Meis1-HdL*. Right figure: N2a cells were transfected with Meis1-HdL and sh-Scramble or sh-*Meis1-all,* and the protein levels were checked by western blotting with an Meis1 antibody. The sh-*Meis1-all* plasmid also knocked down *Meis1-HdL*.

B–D. Immunostaining with GFP (green) and p27 (magenta) in P11 cerebella electroporated with

sh-*Meis1-HdL* and H3.1-EGFP (**B**), sh-*Meis1-HdL*, Res-Meis1-HdL, and H3.1-EGFP (**C**), or sh-*Meis1-all* and H3.1-EGFP(**D**) at P8. Electroporated-cell nuclei were labeled with H3.1-EGFP (green). Scale bar, 20 μm.

Figure 3--figure supplement 2. *Meis1-HdL*-knockdown reduces the ATOH1 fluorescence signal in GCPs.

A–C. Immunostaining with GFP (yellow), KI67 (cyan), and ATOH1 (magenta) in P11 cerebella electroporated with H3.1-EGFP only (**A**), sh-*Meis1-HdL* and H3.1-EGFP (**B**), or sh-*Meis1-all* and H3.1-EGFP(**C**) at P8. Nuclei of electroporated cells were labeled with H3.1-EGFP (yellow). Arrows: electroporated cells; arrowheads, non-electroporated cells.

D, E. Fluorescence intensities of KI67 (**D**) and ATOH1 (**E**) in GFP^+ and GFP^- cells were evaluated by immunostaining with KI67 and ATOH1 antibodies. In the outer EGL, *Meis1*-knockdown did not change the fluorescence intensity of KI67 but reduced that of ATOH1. Scale bar, 20 μm.

Figure 5--figure supplement 1. CUL3 recognizes and degrades S328 phosphorylated ATOH1, which is inhibited by MEIS1.

A. Schematic illustration of proteomic analysis to identify the phosphorylation sites of ATOH1 in the presence or absence of MEIS1.

B. Phosphorylation sites of GST-ATOH1 purified from N2a cells were determined by LC–MS/MS in the presence or absence of MEIS1. Five phosphorylation sites (Y78, S82, S309, S311, and S328) were identified. Phosphorylation of ATOH1-S328 was markedly increased in the presence of MEIS1 (see the attached Data).

C. N2a cells were transfected with GST-Atoh1 alone or in combination with GST-Atoh1, Meis1-FL, or Meis1-HdL. The samples were loaded to contain equal amounts of ATOH1. ATOH1-S328 phosphorylation was determined by western blotting with the ATOH1 p-S328 antibody.

D. N2a cells transfected with GST-Atoh1-S328A (non-phosphorylated form) or GST-Atoh1-S328D (phosphorylated mimic form) plasmids were harvested after 0, 4, and 8 h of treatment with 50 μg/mL cycloheximide (Chx). The lysates were immunoblotted with anti-ATOH1 or GAPDH.

E. N2a cells transfected with GST-Atoh1-S328D in combination with Meis1-FL or Meis1-HdL plasmids were harvested after 0, 4, and 8 h treatment with 50 μg/mL Chx. The lysates were immunoblotted with anti-ATOH1 or GAPDH.

F. ATOH1 levels relative to those of GAPDH in **d** and **e**. Mean ± SEM from three trials of each condition.

G. N2a cells were transfected with HA-Ub in combination with GST-Atoh1 or GST-Atoh1-S328A. After GST pull-down, ATOH1 ubiquitination and total ATOH1 levels were determined by immunoblotting with anti-HA and anti-GST antibodies. The interaction of CUL3 with GST-ATOH1 was determined by immunoblotting with an anti-CUL3 antibody.

Figure 5--figure supplement 2. BMP-ERK signaling phosphorylates Ser328 of ATOH1, thereby inducing CULLIN-dependent ATOH1 degradation.

A. N2a cells were transfected with GST-Atoh1 and cultured for 48 h. Other N2a cells were treated with the indicated inhibitors for 24 h and with MG132 for 6 h, before harvesting. After GST pull-down, ATOH1 phosphorylation (upper panel) and total ATOH1 levels (lower panel) were determined by immunoblotting with anti-ATOH1 p-S328 and anti-ATOH1 antibodies. Treatment with SCH772984 (an ERK inhibitor) reduced ATOH1 S328 phosphorylation.

B. ERK1 kinase assay performed with purified recombinant ERK1 incubated with MBP-ATOH1 substrate. Phosphorylation of S328 in the MBP-ATOH1 substrate was detected with ATOH1 p-S328 antibody.

C. Purified P6 GCPs were incubated for 48 h. Six hours before cell harvest, MG132 alone or in combination with BMP4 was administered. ATOH1 phosphorylation was determined using western blotting with ATOH1 p-S328 and ATOH1 antibodies. BMP administration raised ATOH1 phosphorylation.

D. Purified P6 GCPs were incubated for 48 h. Six hours before cell harvest, MG132 alone, MG132 with BMP4, or MG132 with BMP4 and MLN4924, were administered. Protein levels were determined using western blotting with the ATOH1 antibody. The reduction in ATOH1 levels due to BMP4 was restored by MLN4924 or MG132 treatment.

E. ATOH1 levels relative to those of GAPDH in **K**. Mean ± SEM from three trials of each condition.

Figure 6--figure supplement 1. MEIS1 stabilizes not only ATOH1 but also other target proteins of CUL3.

A. Schematic of proteomic analysis to identify MEIS1 binding molecules.

B. N2a cells were transfected with HA-Cops6 and GST, GST-Meis1 1–130 aa, GST-Meis1-HdL, or GST-Meis1-FL. After GST pull-down, the interaction of HA-COPS6 with GST-tagged protein was determined by immunoblotting with anti-HA and anti-GST antibodies. HA-COPS6 did not bind to GST and GST-MEIS1 1–130 aa.

C. N2a cells were transfected with HA-Cops6 and Meis1-FL or Meis1-HdL and sh-Scramble or sh-*Cul3*. After immunoprecipitation with an HA antibody, the interactions of MEIS1-FL or MEIS1-HdL with CUL3 and HA-COPS6 were determined by immunoblotting with anti-HA,

anti-CUL3, and anti-MEIS1 antibodies. MEIS1 and COPS6 were able to bind without CUL3.

D. N2a cells were transfected with HA-Cops6 and sh-Scramble, sh-*Cops6-1*, or sh-*Cops6-2* plasmids. Protein levels were determined by western blotting with HA antibody. The sh-*Cops6-1* and sh-*Cops6-2* plasmids efficiently knocked down *Cops6*.

E. Immunoblotting with the indicated CUL3 target protein antibodies (NRF2, NCOA3, PP2A/C) on lysates from N2a cells transfected with Meis1-FL, Meis1-HdL, or empty vector plasmids. At 48 h after transfection, cells were treated with or without MG132 for 6 h. MG132 treatment or Meis1 overexpression stabilized the target proteins of CUL3.

F–H. N2a cells were transfected with HA-Cops6 alone (**F**) or with HA-Cops6 and Meis1-FL-EGFP (**G**) or Meis1-HdL-EGFP (**H**) and immunostained for HA (magenta, **G–H**), GFP (green, **G**, and **H**), and DAPI (blue). HA-COPS6 signal localization was not altered in the presence of MEIS1-FL or MEIS1-HdL. Scale bar, 10 μm.

Figure 1

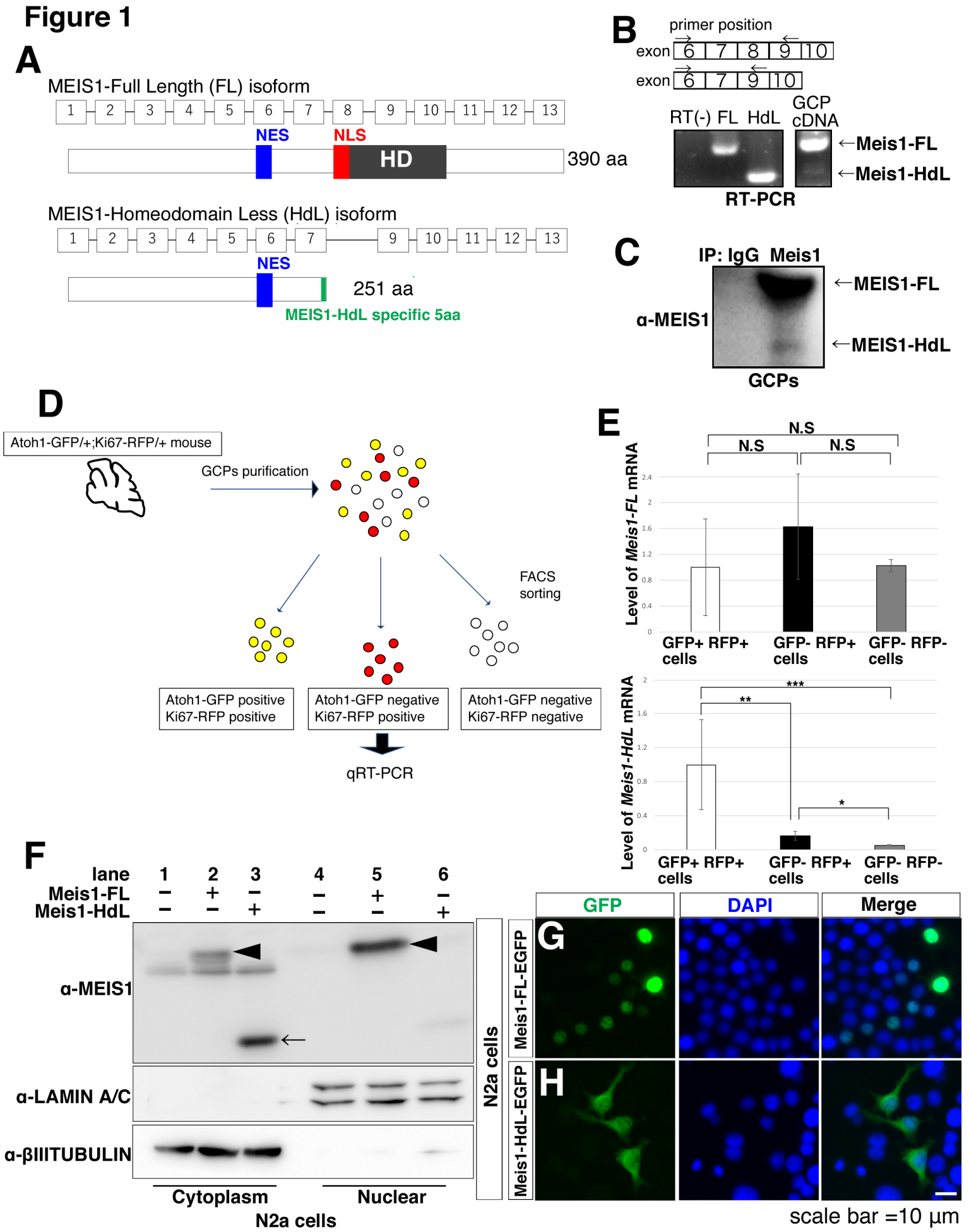
A
MEIS1-Full Length (FL) isoform
1 2 3 4 5 6 7 8 9 10 11 12 13
NES
NLS
HD
390 aa
MEIS1-Homeodomain Less (HdL) isoform
1 2 3 4 5 6 7 9 10 11 12 13
NES
251 aa
MEIS1-HdL specific 5aa
B
primer position
exon 6 7 8 9 10
exon 6 7 9 10
RT(-) FL HdL
GCP cDNA
←Meis1-FL
←Meis1-HdL
RT-PCR
C
IP: IgG Meis1
α-MEIS1
←MEIS1-FL
←MEIS1-HdL
GCPs
D
Atoh1-GFP/+;Ki67-RFP/+ mouse
GCPs purification
FACS sorting
Atoh1-GFP positive Ki67-RFP positive
Atoh1-GFP negative Ki67-RFP positive
Atoh1-GFP negative Ki67-RFP negative
qRT-PCR
E
N.S
N.S
N.S
Level of Meis1-FL mRNA
GFP+ RFP+ cells
GFP- RFP+ cells
GFP- RFP- cells
Level of Meis1-HdL mRNA
***
**
*
F
lane 1 2 3 4 5 6
Meis1-FL − + − − + −
Meis1-HdL − − + − − +
α-MEIS1
α-LAMIN A/C
α-βIIITUBULIN
Cytoplasm
Nuclear
N2a cells
N2a cells
Meis1-FL-EGFP
Meis1-HdL-EGFP
GFP
DAPI
Merge
G
H
scale bar =10 μm

Figure 2

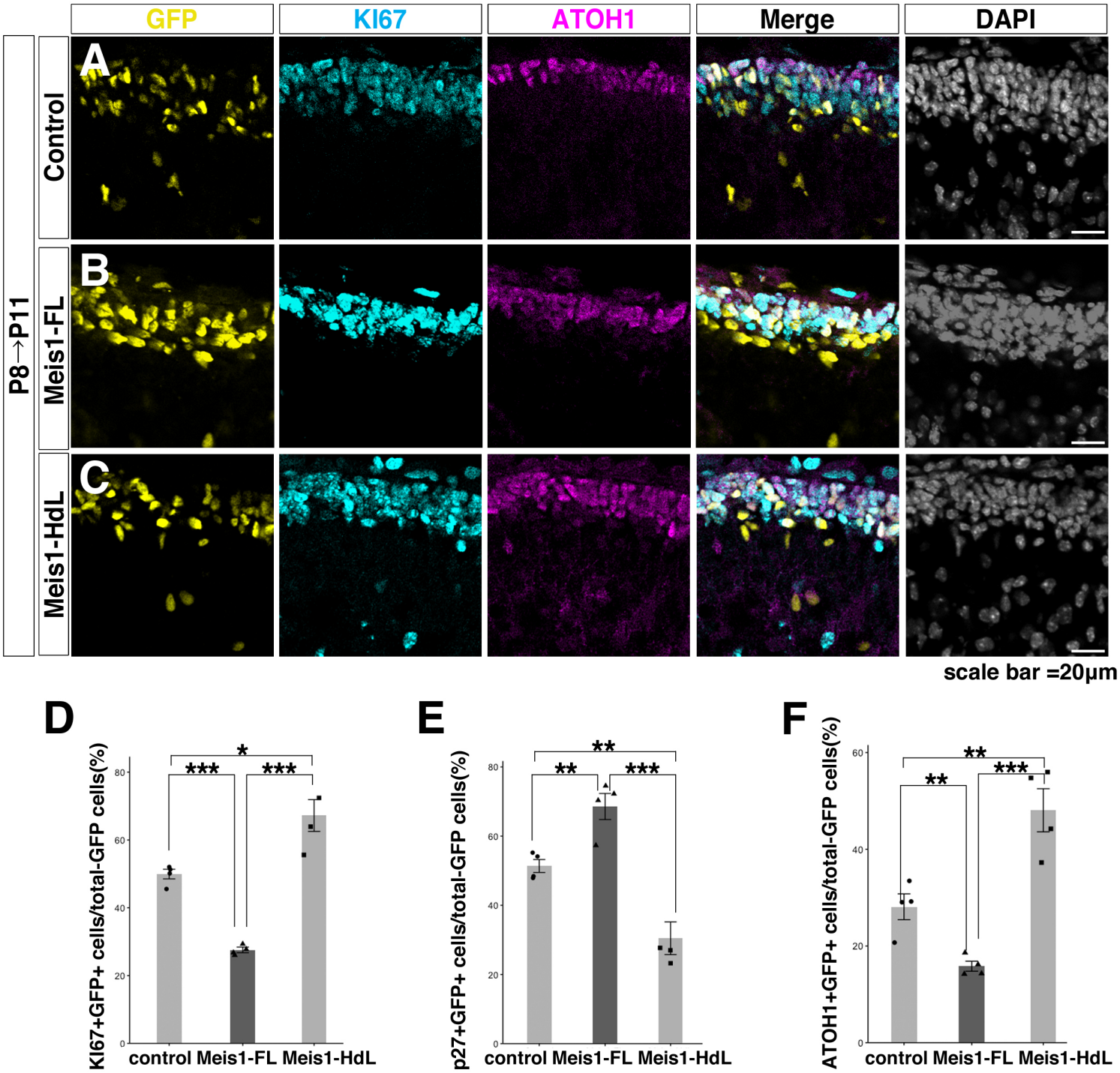
GFP
KI67
ATOH1
Merge
DAPI
P8→P11
Control
Meis1-FL
Meis1-HdL
A
B
C
scale bar =20μm
D
KI67+GFP+ cells/total-GFP cells(%)
control Meis1-FL Meis1-HdL
E
p27+GFP+ cells/total-GFP cells(%)
control Meis1-FL Meis1-HdL
F
ATOH1+GFP+ cells/total-GFP cells(%)
control Meis1-FL Meis1-HdL

Figure 3

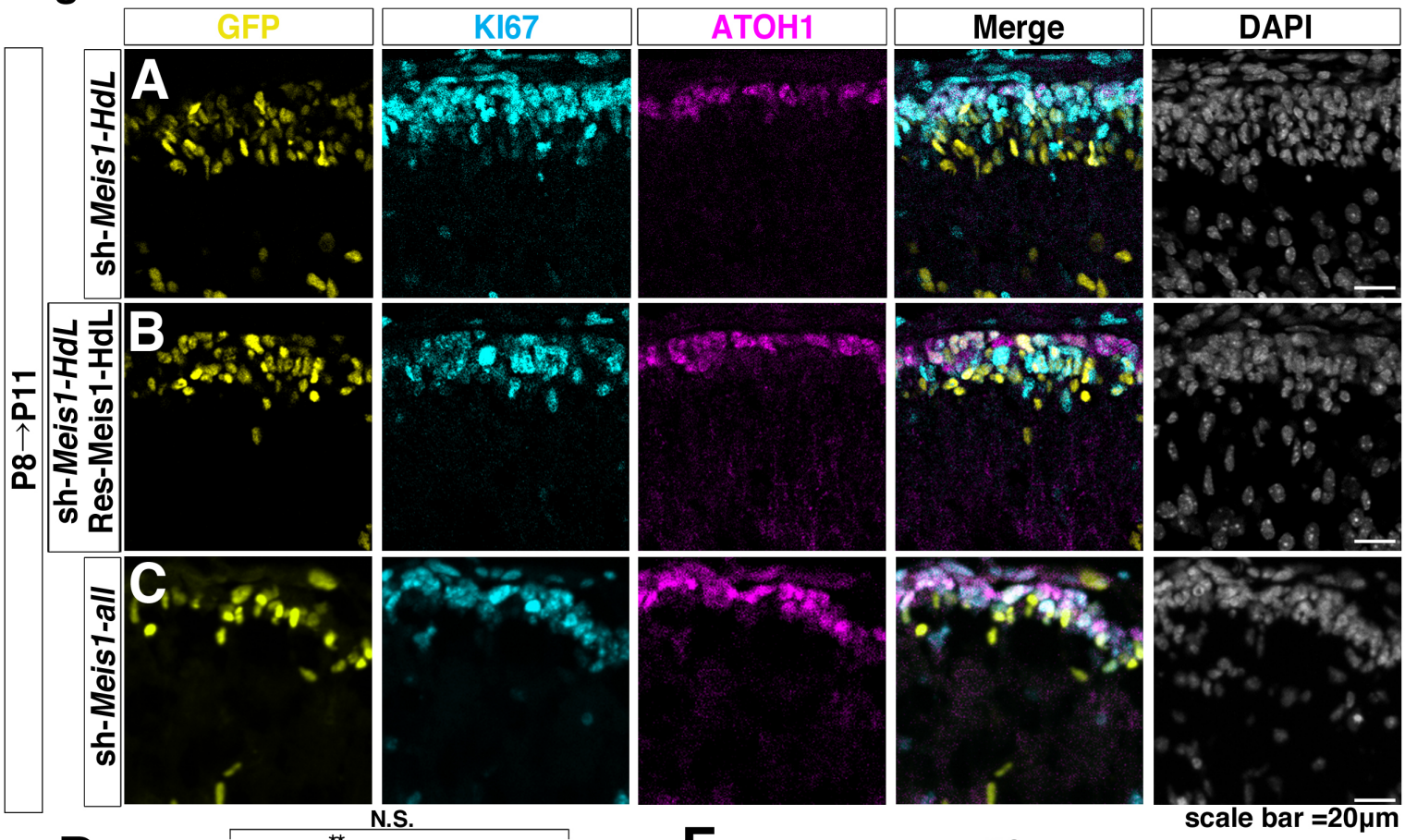
GFP
KI67
ATOH1
Merge
DAPI
P8→P11
A
sh-Meis1-HdL
B
sh-Meis1-HdL
Res-Meis1-HdL
C
sh-Meis1-all
scale bar =20μm

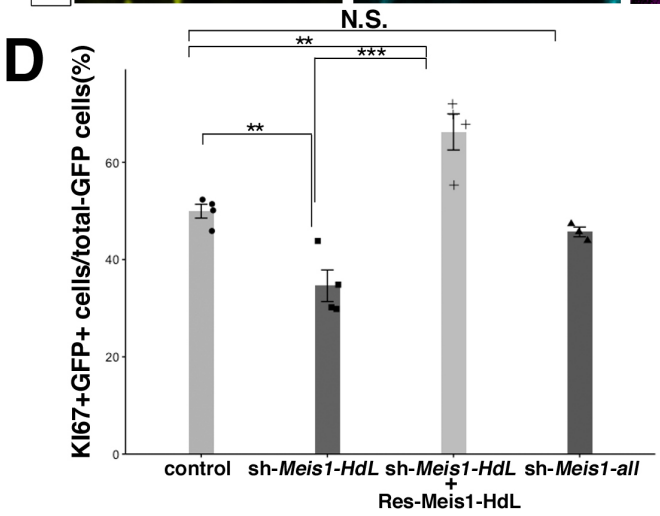
D
N.S.
**
***
**
KI67+GFP+ cells/total-GFP cells(%)
0
20
40
60
control
sh-Meis1-HdL
sh-Meis1-HdL + Res-Meis1-HdL
sh-Meis1-all

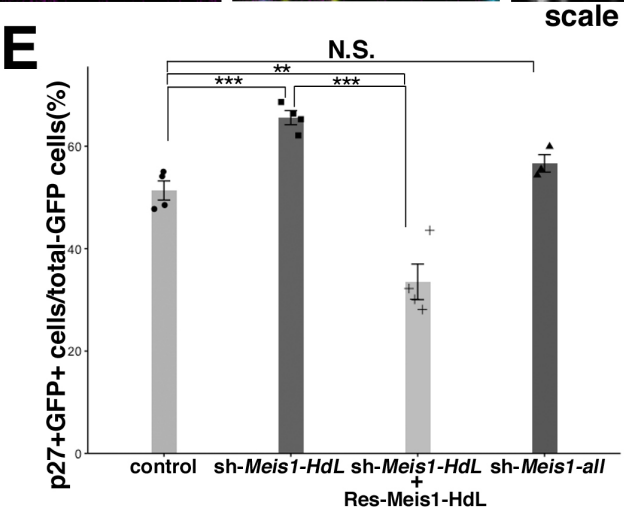
E
N.S.
**
***
***
p27+GFP+ cells/total-GFP cells(%)
0
20
40
60
control
sh-Meis1-HdL
sh-Meis1-HdL + Res-Meis1-HdL
sh-Meis1-all

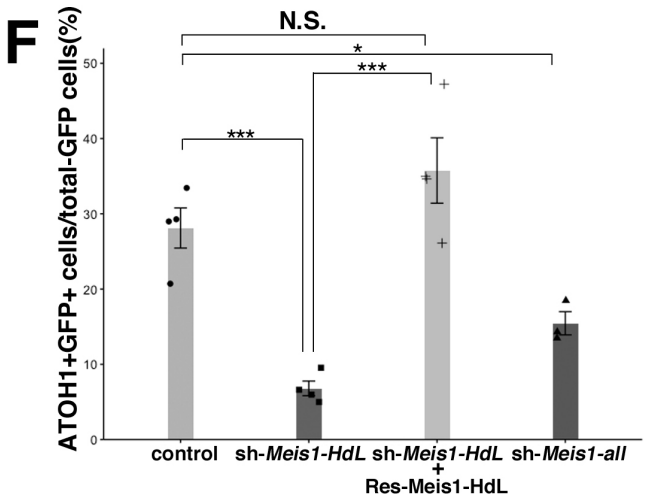
F
N.S.
*
***
***
ATOH1+GFP+ cells/total-GFP cells(%)
0
10
20
30
40
50
control
sh-Meis1-HdL
sh-Meis1-HdL + Res-Meis1-HdL
sh-Meis1-all

Figure 4

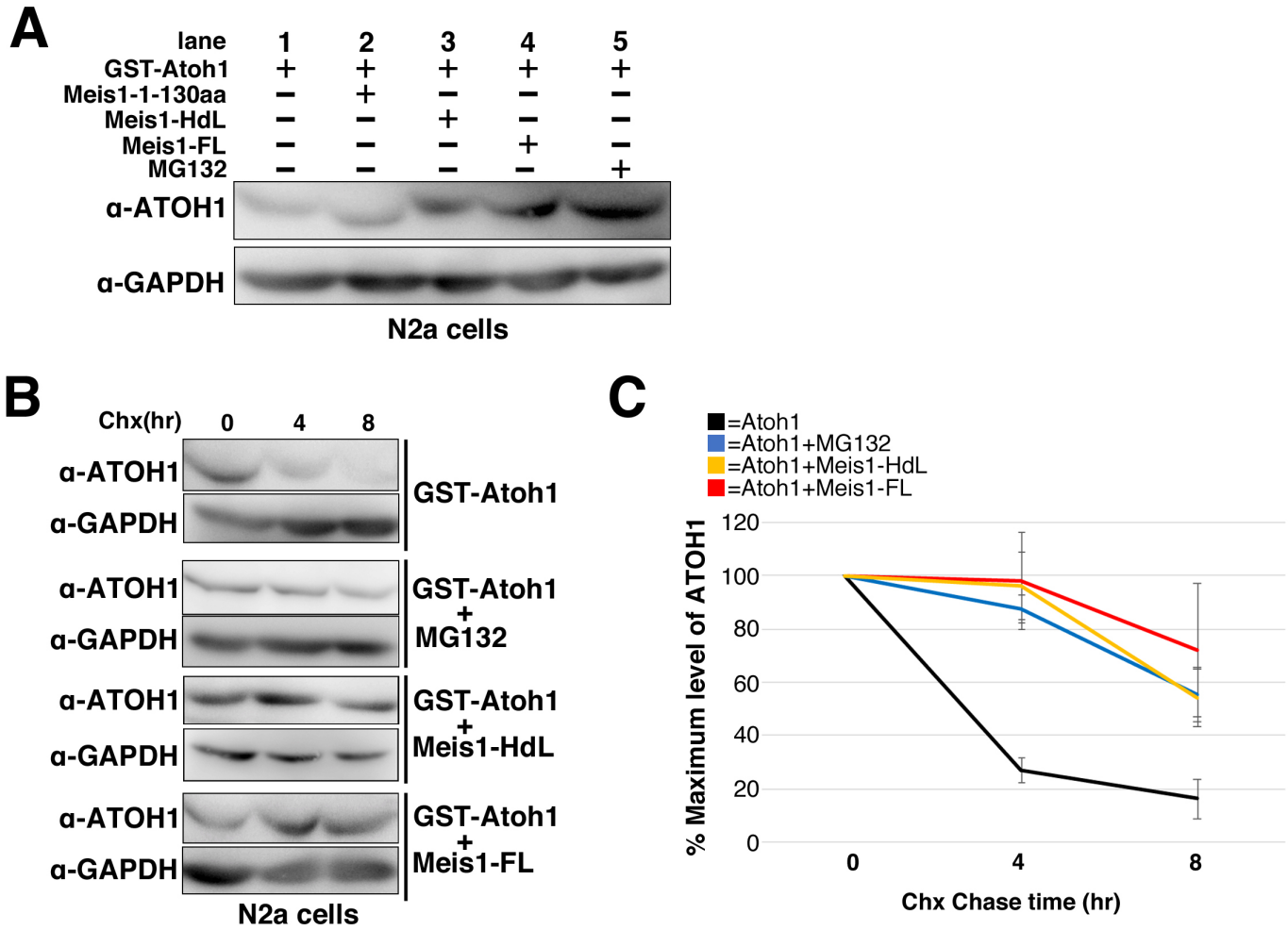
A
lane 1 2 3 4 5
GST-Atoh1 + + + + +
Meis1-1-130aa − + − − −
Meis1-HdL − − + − −
Meis1-FL − − − + −
MG132 − − − − +
α-ATOH1
α-GAPDH
N2a cells
B
Chx(hr) 0 4 8
α-ATOH1
α-GAPDH
GST-Atoh1
GST-Atoh1 + MG132
GST-Atoh1 + Meis1-HdL
GST-Atoh1 + Meis1-FL
N2a cells
C
=Atoh1
=Atoh1+MG132
=Atoh1+Meis1-HdL
=Atoh1+Meis1-FL
% Maximum level of ATOH1
120
100
80
60
40
20
0
0
4
8
Chx Chase time (hr)

Figure 5

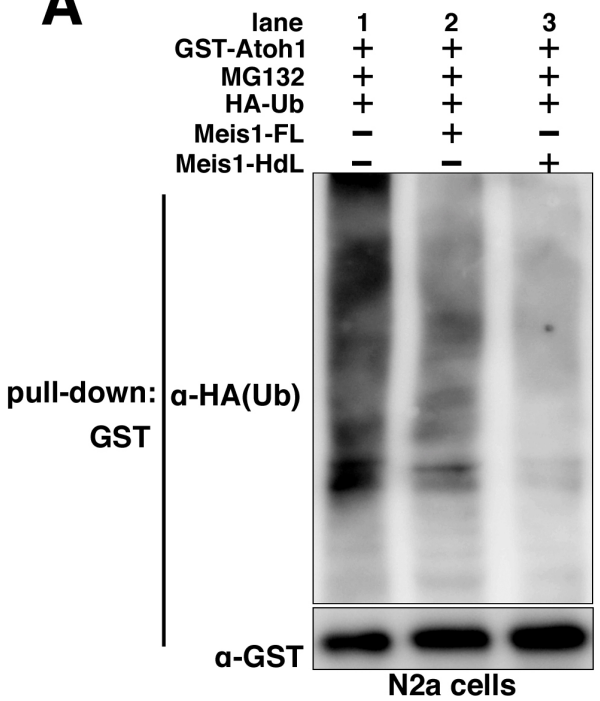

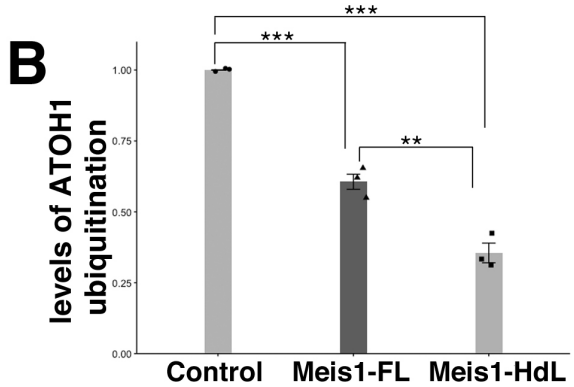

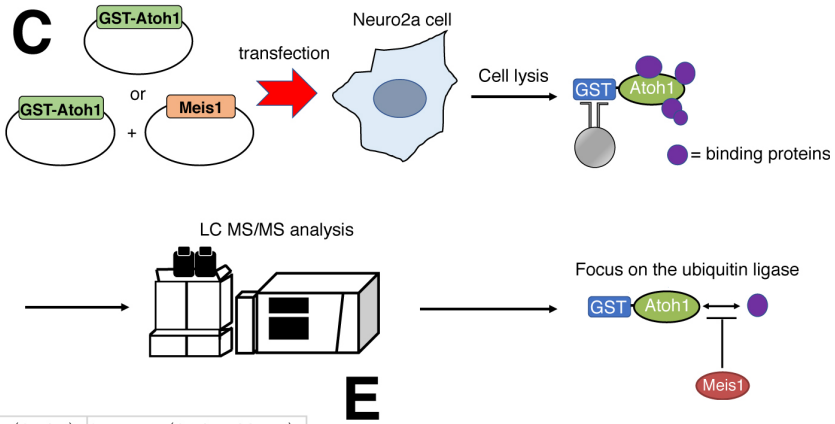

D

Gene name		Intensity (Atoh1)	Intensity (Atoh1+Meis1)
Aktip	AKT-interacting protein	352070	152570
Cand1	Cullin-associated NEDD8-dissociated protein 1	2627800	695510
Cul3	Cullin-3	243480	0
Uba1	Ubiquitin-like modifier-activating enzyme 1	3634600	1198000
Ube2m	NEDD8-conjugating enzyme Ubc12	583210	146110
Ube2n	Ubiquitin-conjugating enzyme E2 N	740660	152830
Ube2t	Ubiquitin-conjugating enzyme E2 T	136410	61796

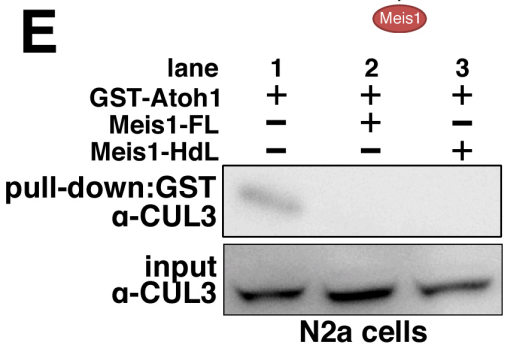

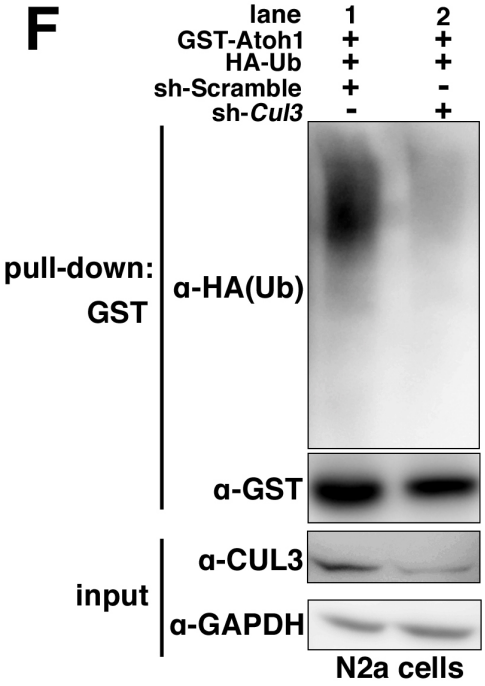

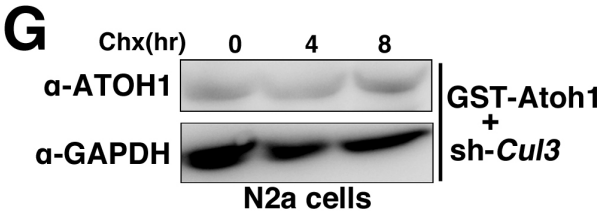

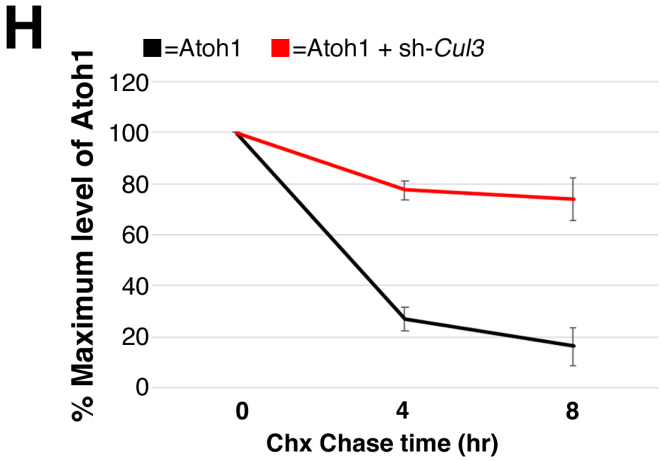

Figure 6

A

Gene name		Intensity(Meis1)
COP9 signalosome complex subunit 2	*Cops2*	2137700
COP9 signalosome complex subunit 3	*Cops3*	1981400
COP9 signalosome complex subunit 4	*Cops4*	4464600
COP9 signalosome complex subunit 6	*Cops6*	2429900
COP9 signalosome complex subunit 7a	*Cops7a*	336880
COP9 signalosome complex subunit 8	*Cops8*	977510

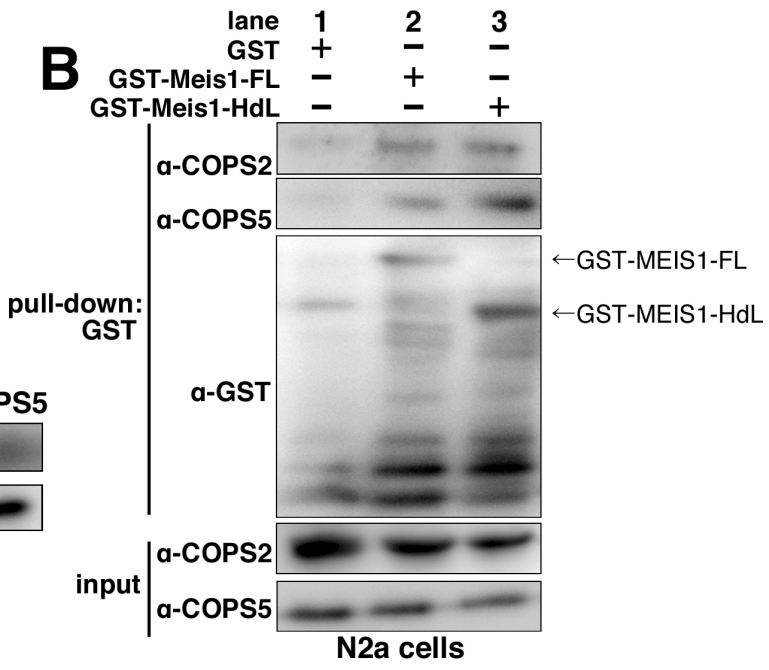

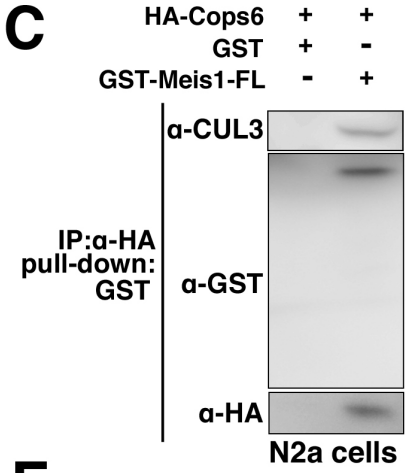

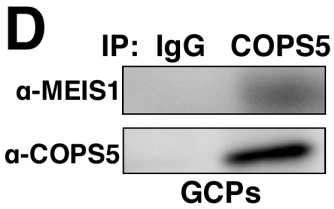

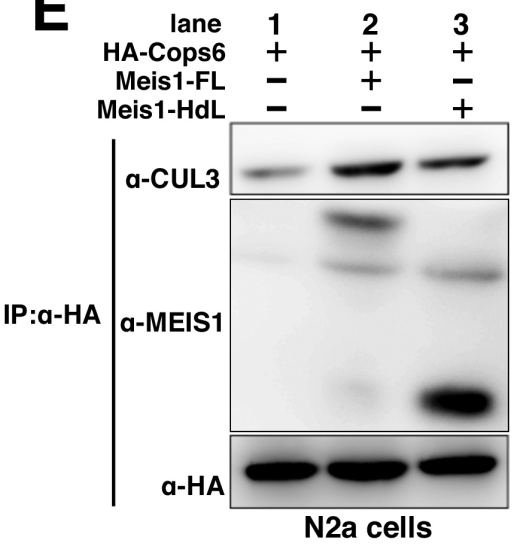

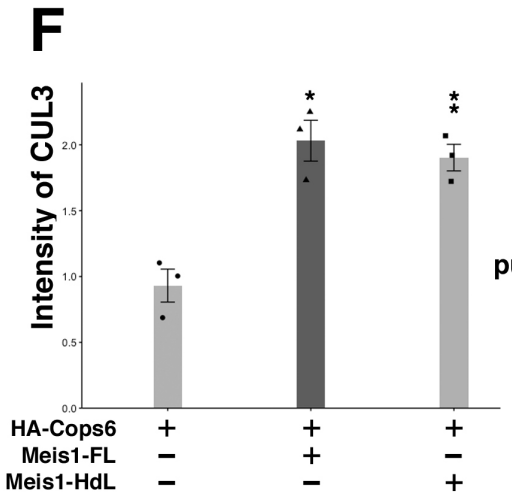

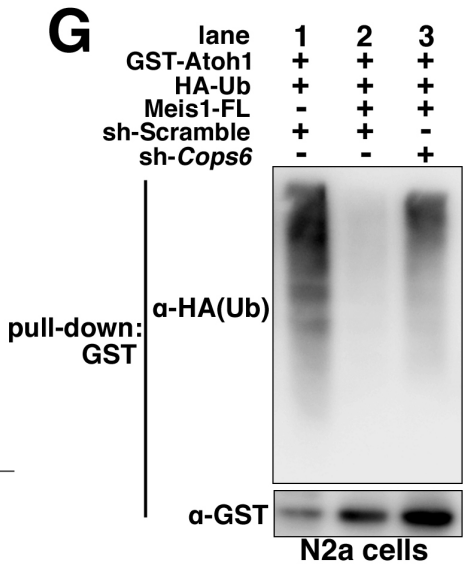

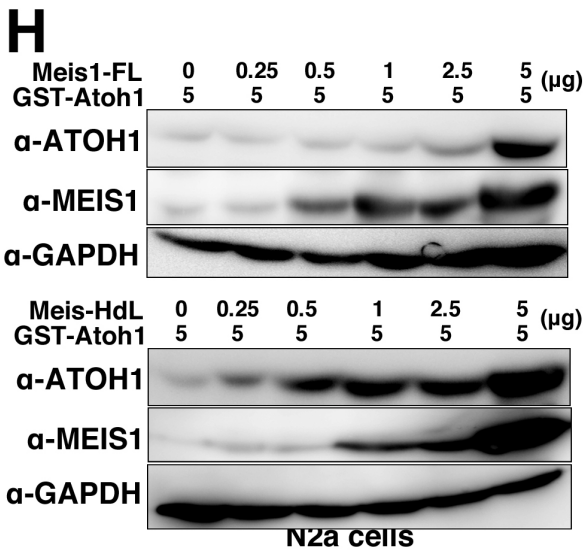

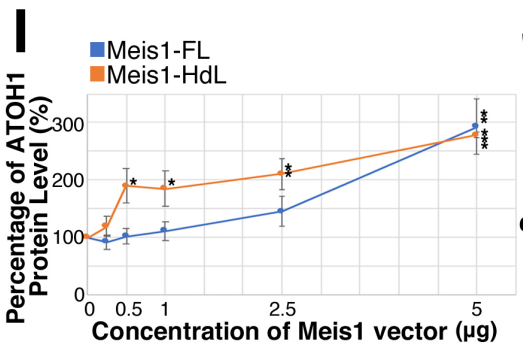

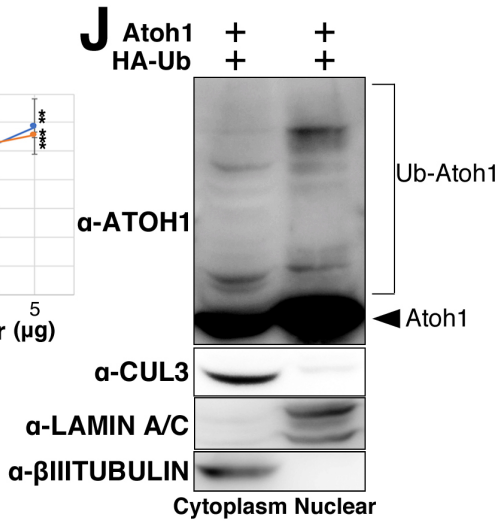

Figure 7

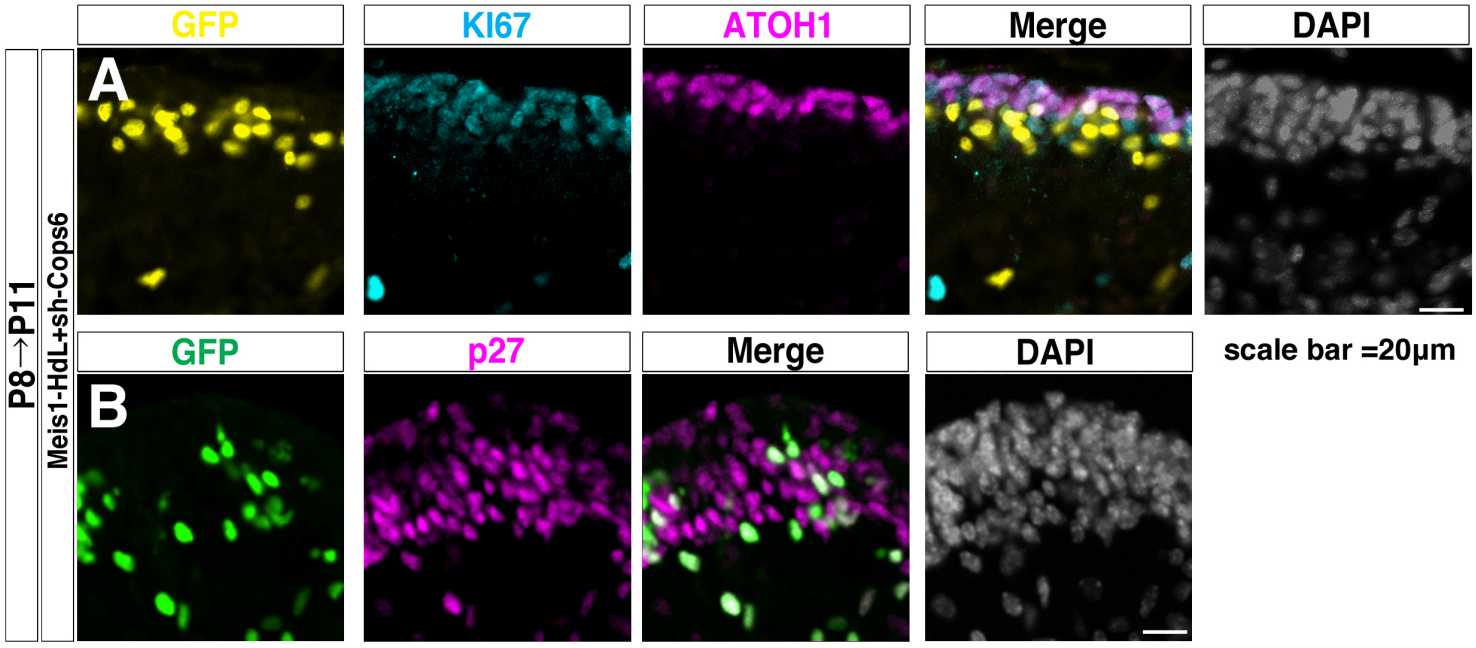
P8→P11
Meis1-HdL+sh-Cops6
A
GFP
KI67
ATOH1
Merge
DAPI
B
GFP
p27
Merge
DAPI
scale bar =20μm

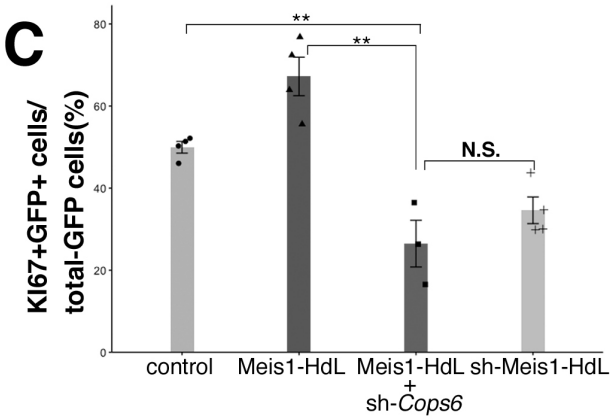
C
KI67+GFP+ cells/
total-GFP cells(%)
**
**
N.S.
control
Meis1-HdL
Meis1-HdL
+
sh-Cops6
sh-Meis1-HdL

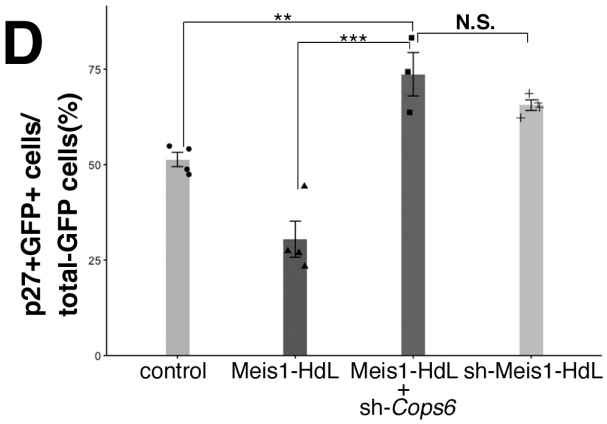
D
p27+GFP+ cells/
total-GFP cells(%)
**
***
N.S.
control
Meis1-HdL
Meis1-HdL
+
sh-Cops6
sh-Meis1-HdL

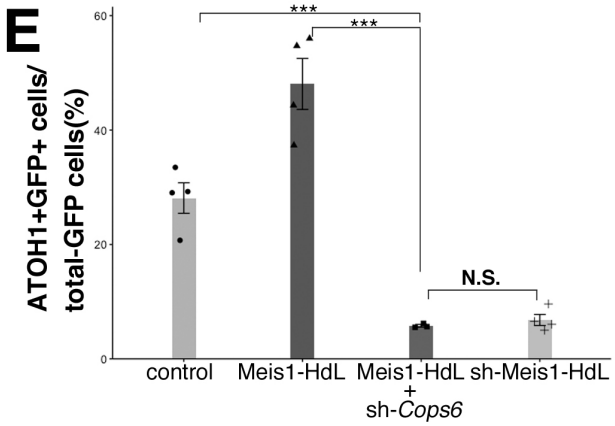
E
ATOH1+GFP+ cells/
total-GFP cells(%)
***
***
N.S.
control
Meis1-HdL
Meis1-HdL
+
sh-Cops6
sh-Meis1-HdL

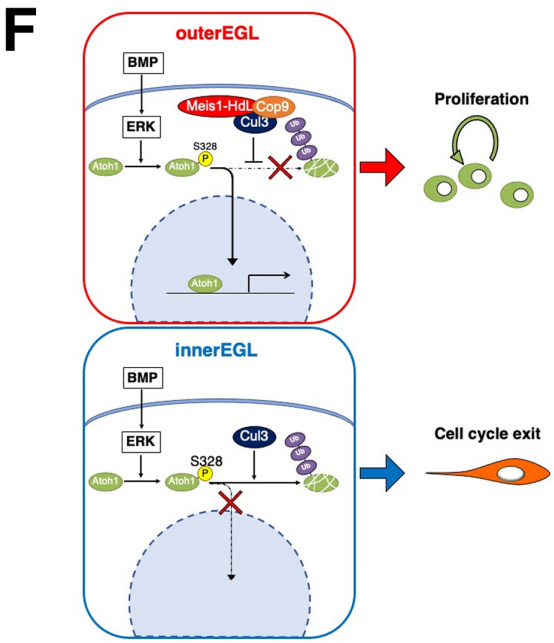
F
outerEGL
BMP
ERK
Meis1-HdL Cop9
Cul3
S328
Atoh1
Proliferation
innerEGL
BMP
ERK
Cul3
S328
Atoh1
Cell cycle exit

Figure 1-figure supplement 1

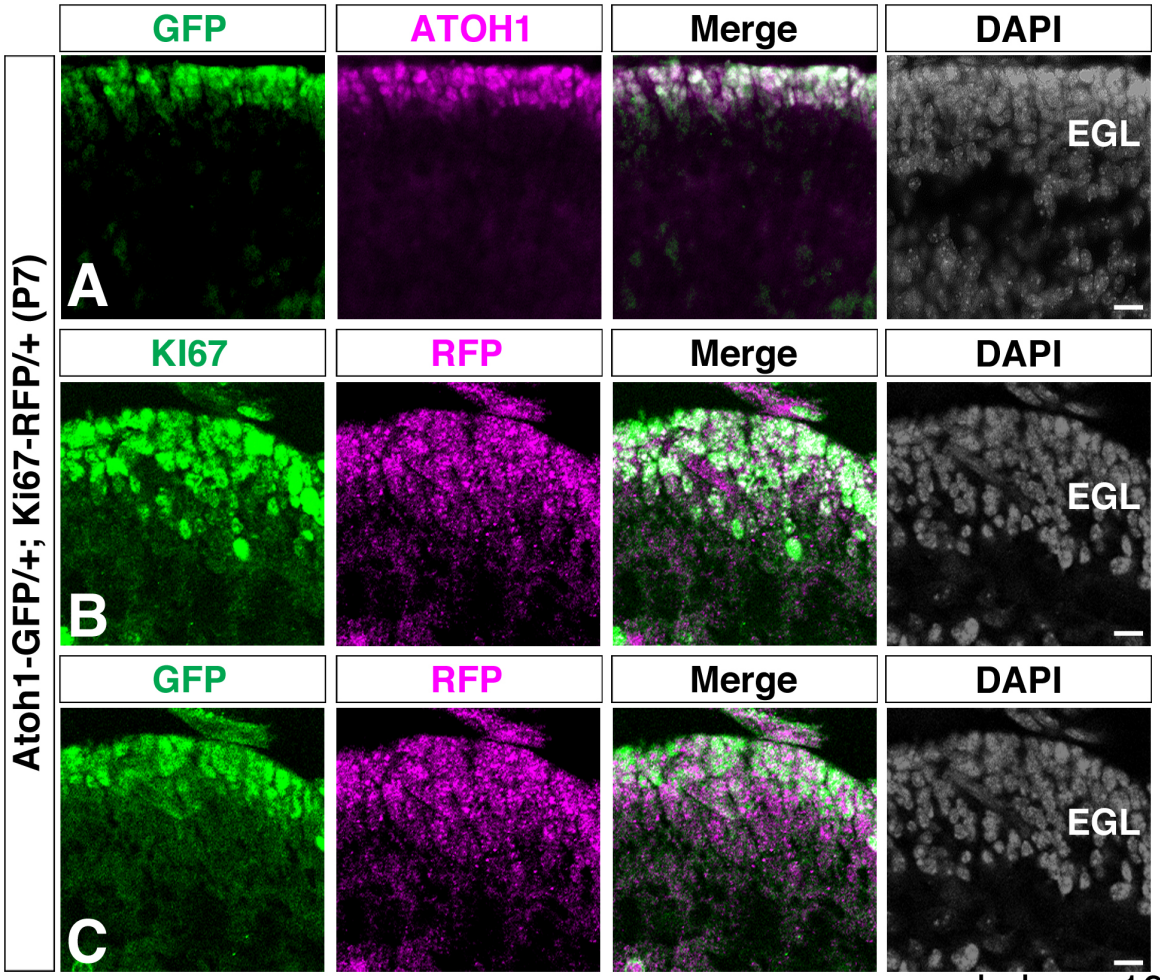

scale bar =10 μm

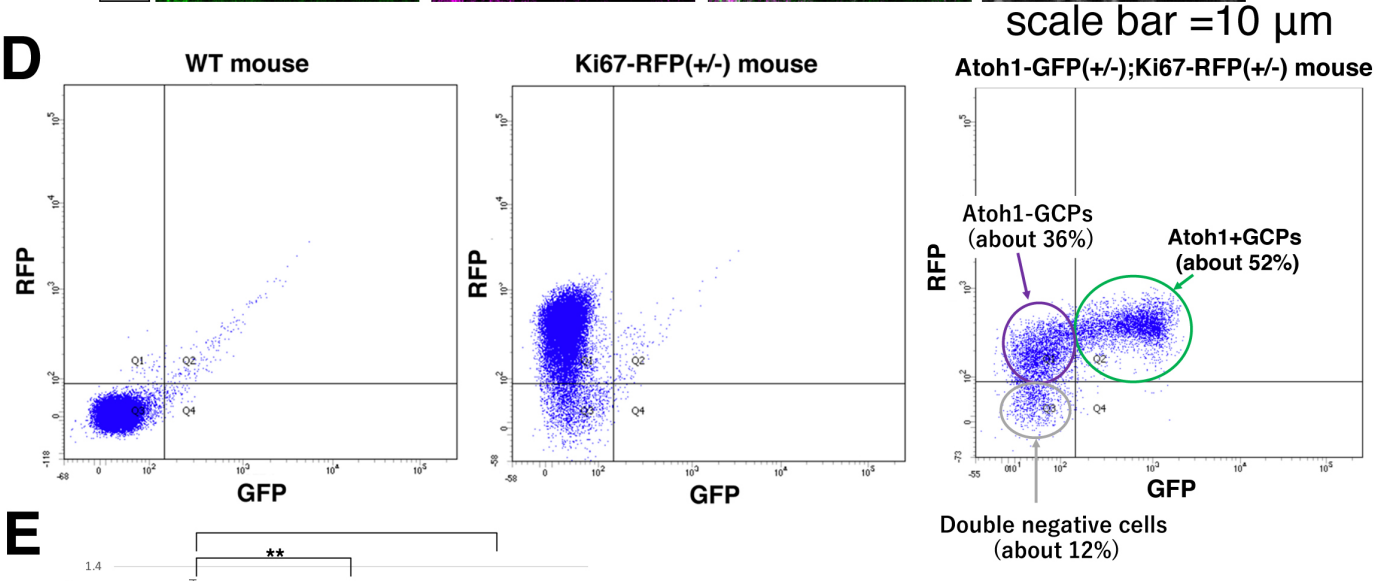

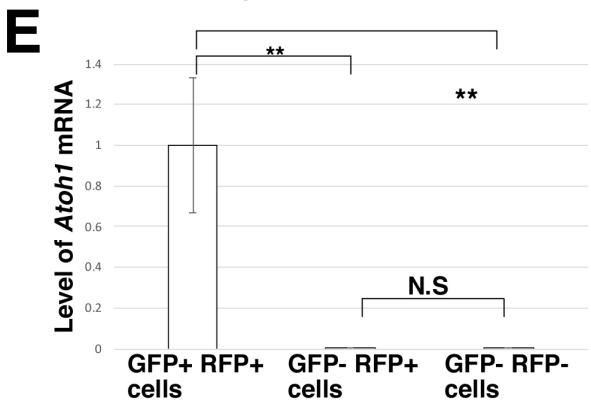

Figure 2-figure supplement 1

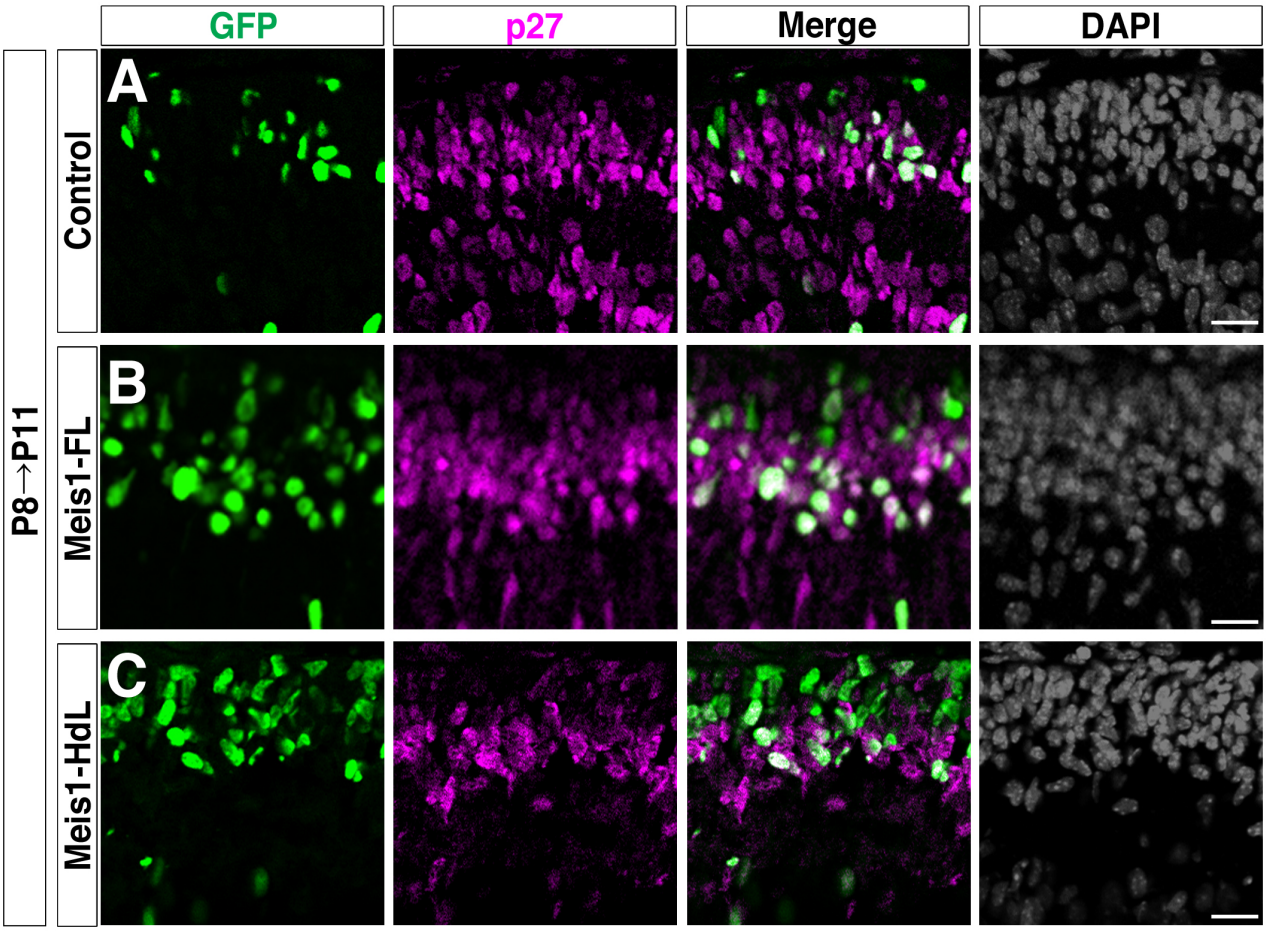

scale bar =20μm

Figure 3-figure supplement 1

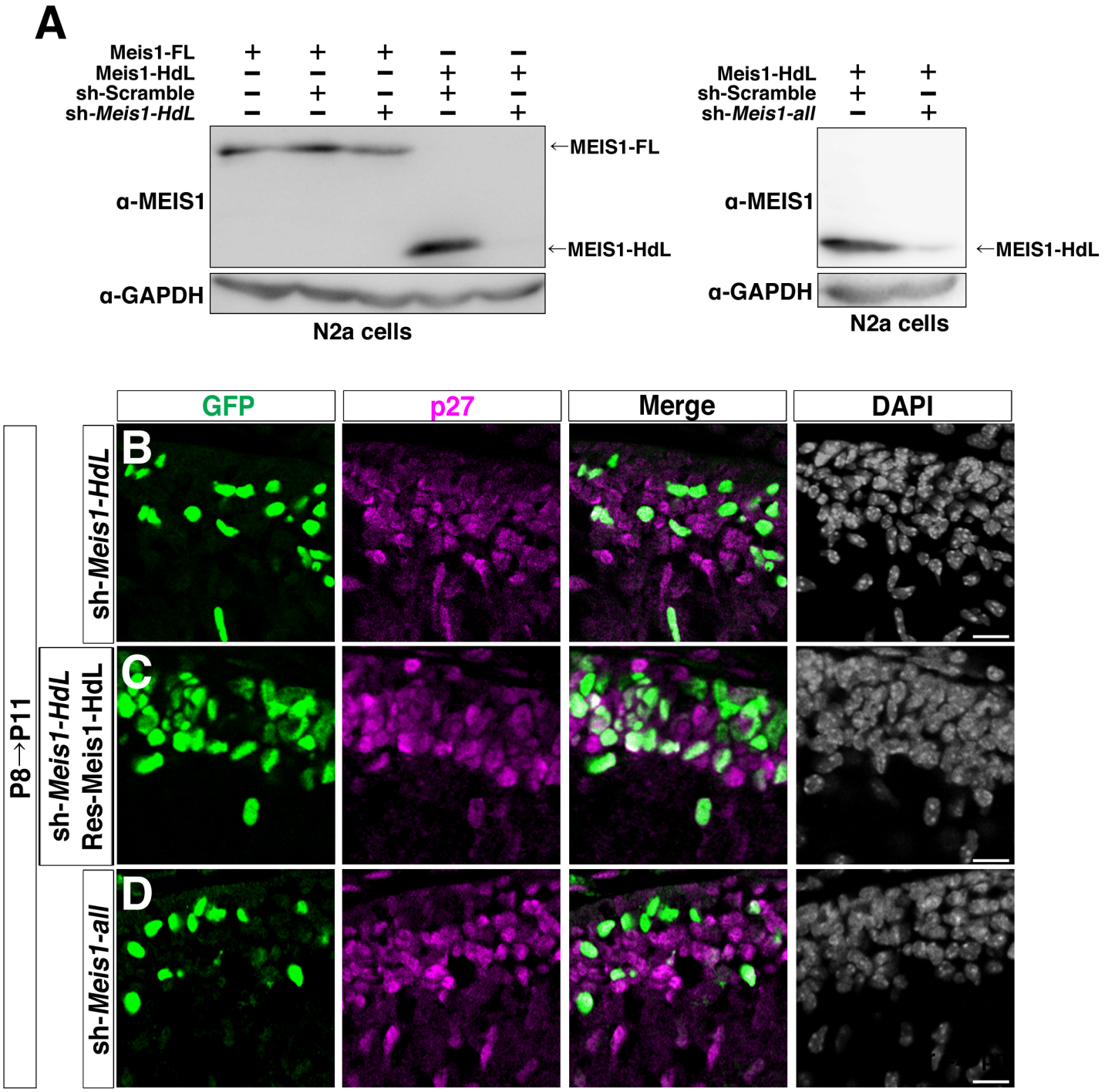

Figure 3-figure supplement 2

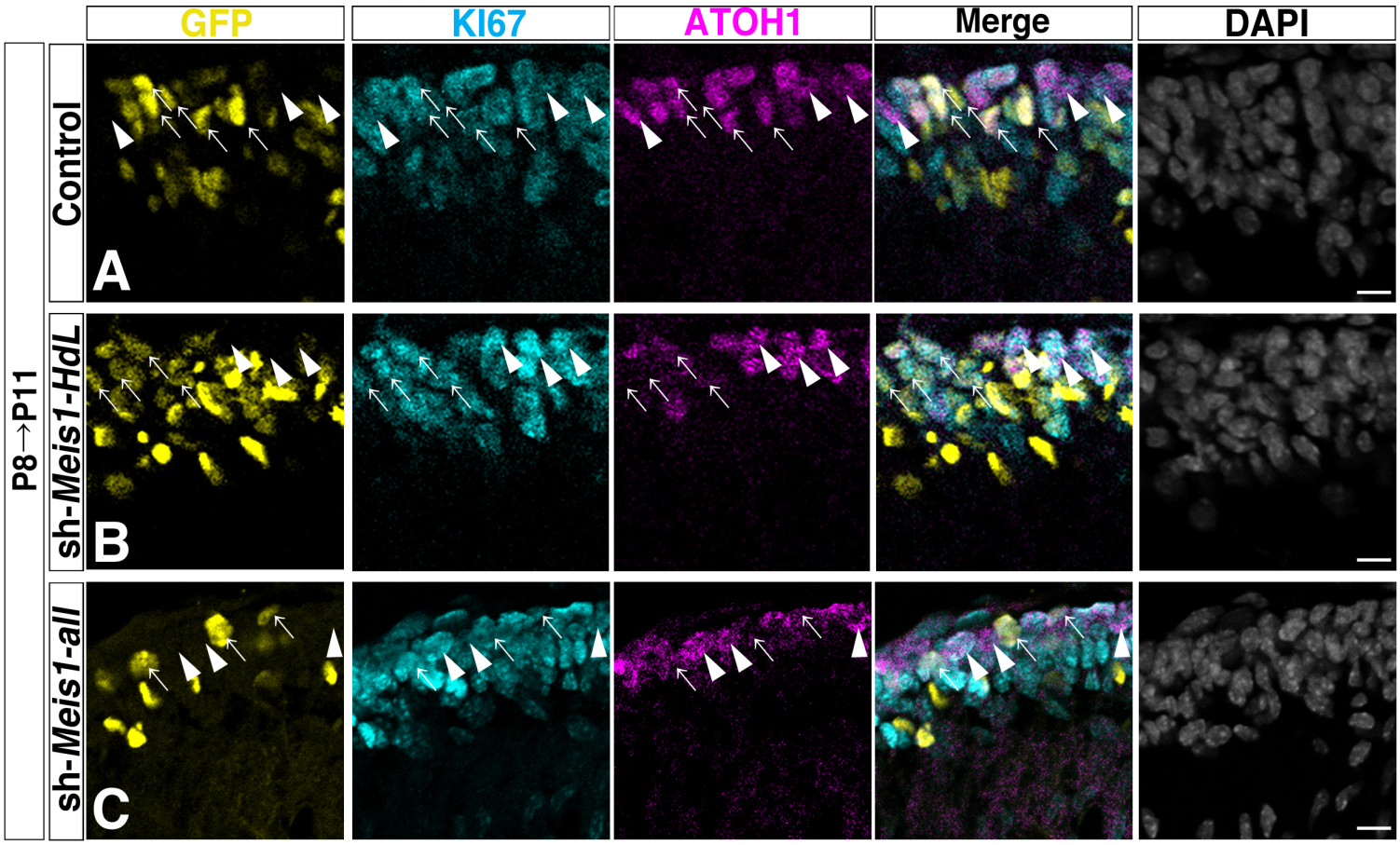

scale bar =20μm

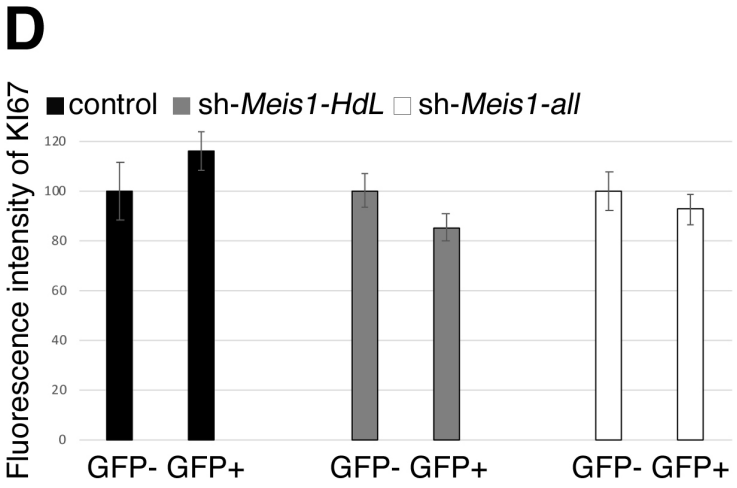

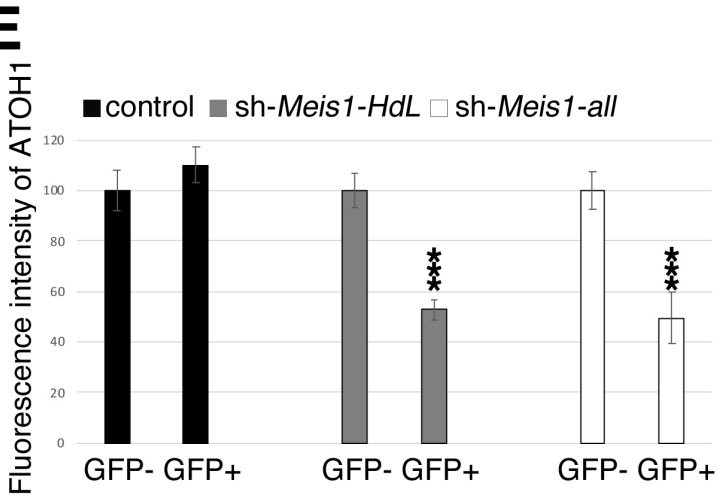

Figure 5-figure supplement 1

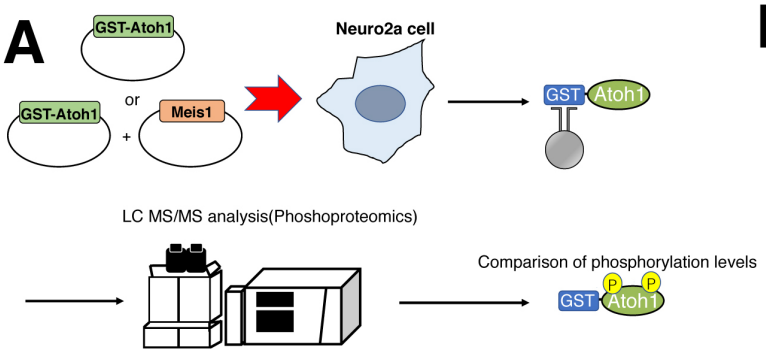

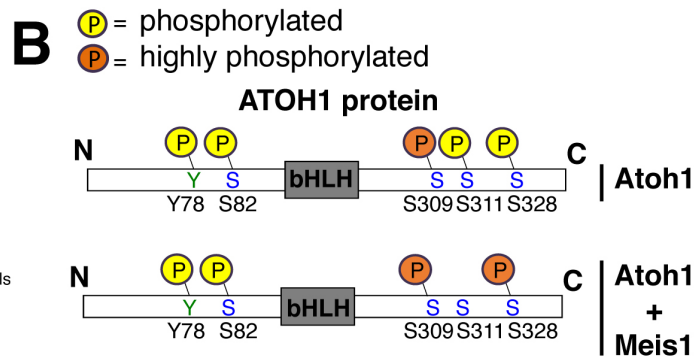

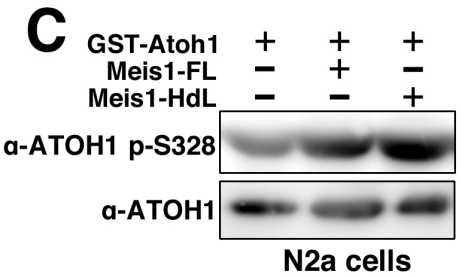

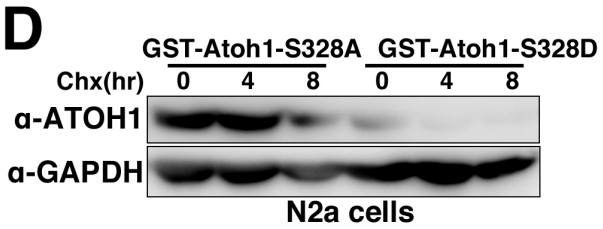

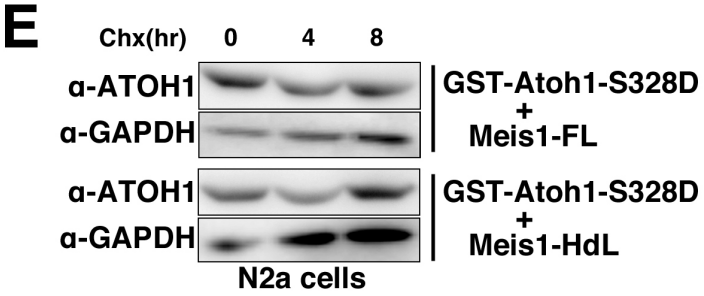

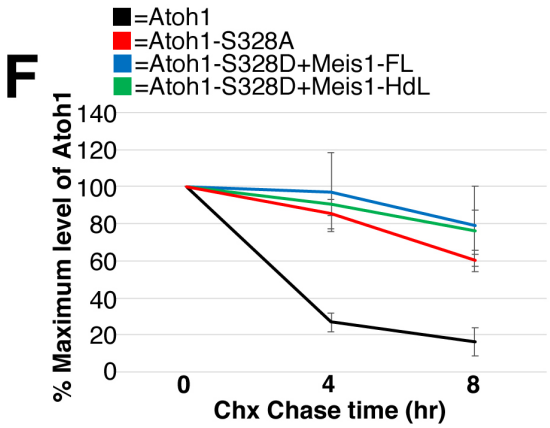

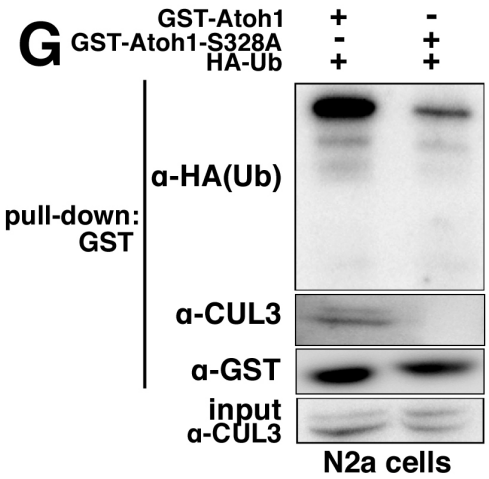

Figure 5-figure supplement 2

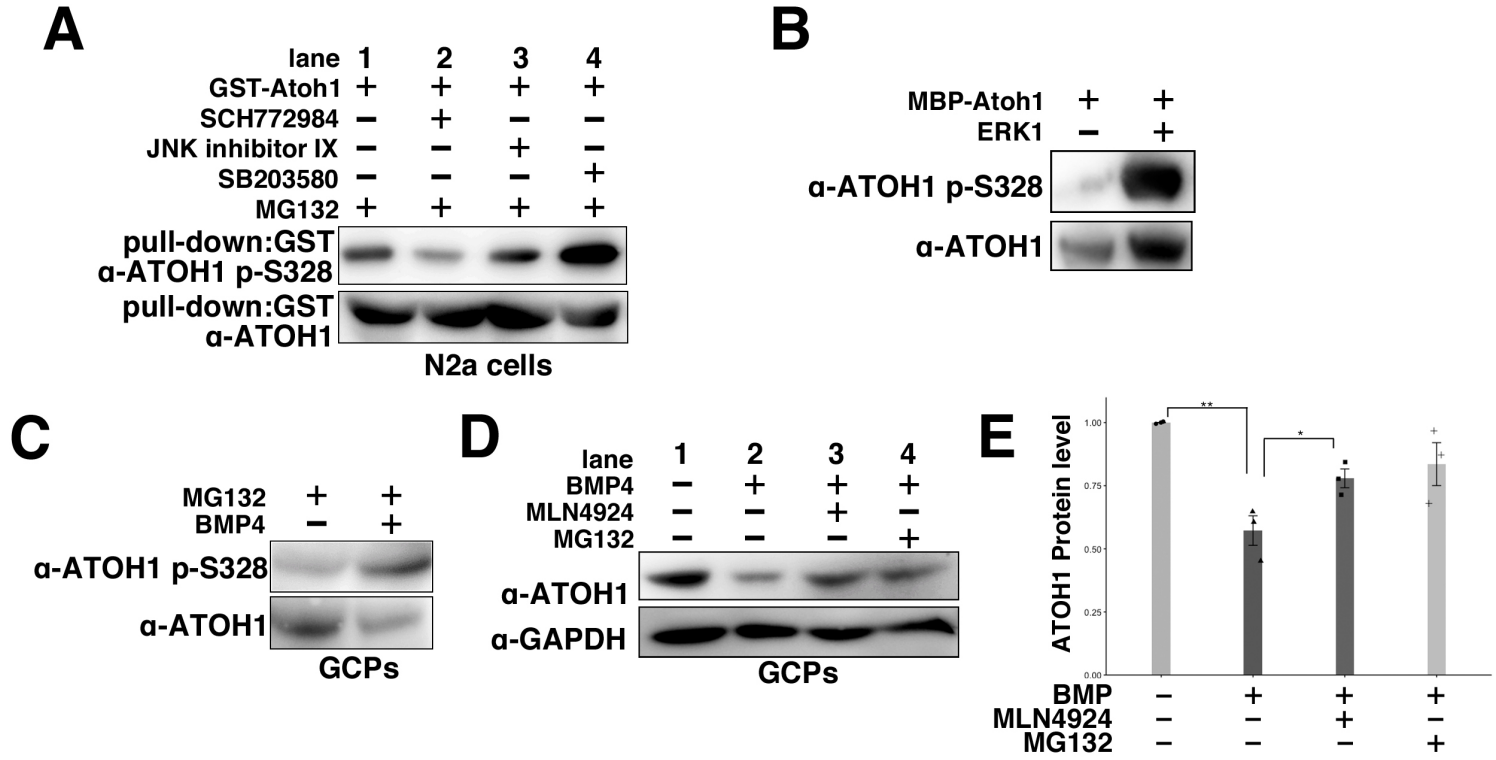
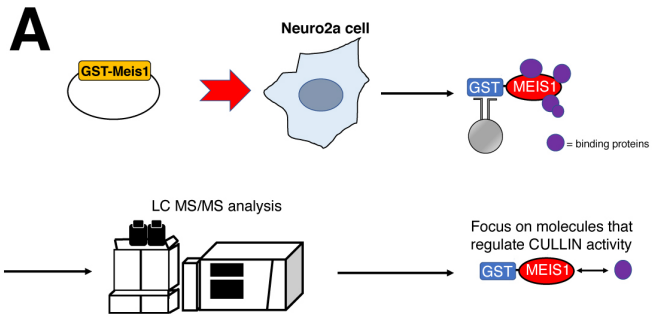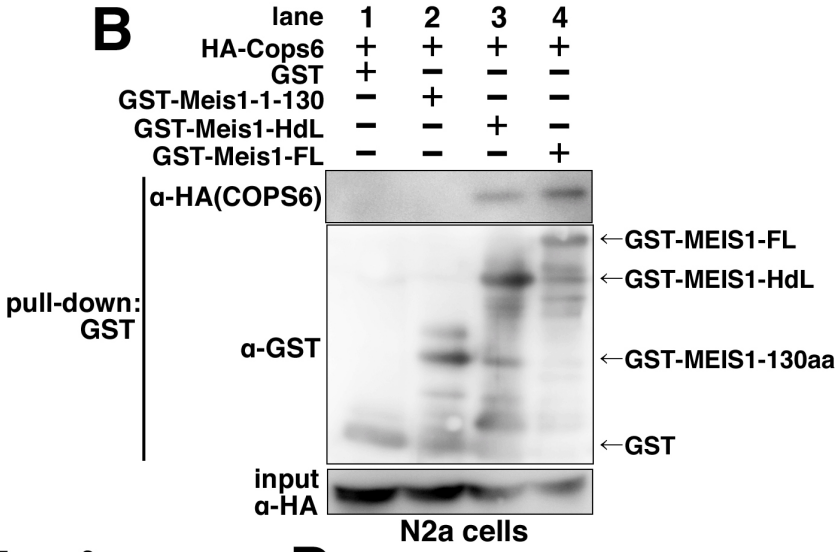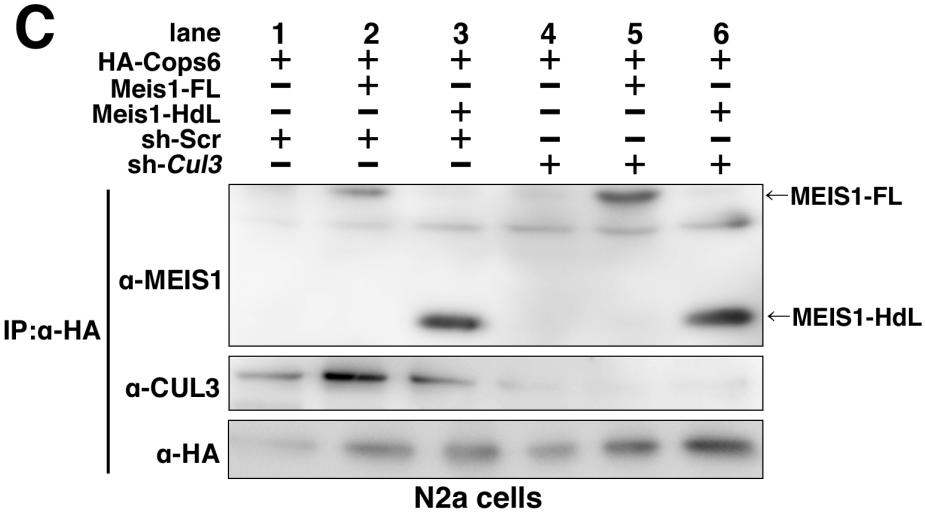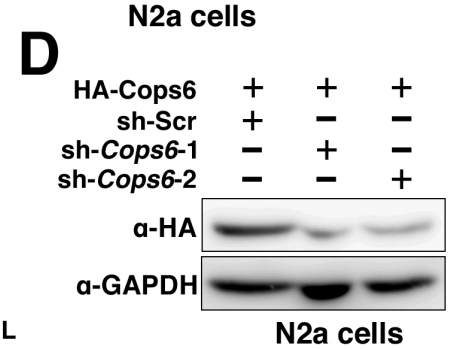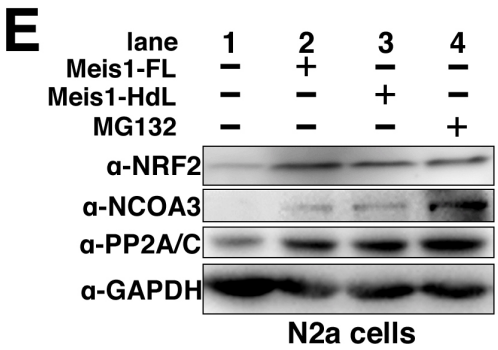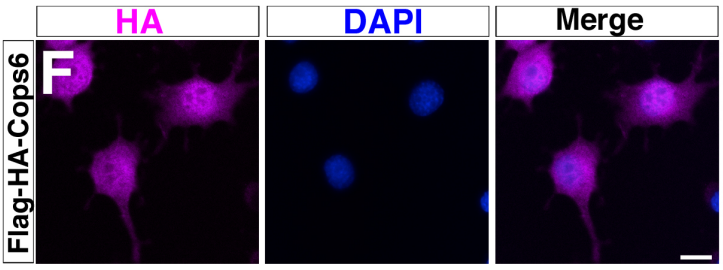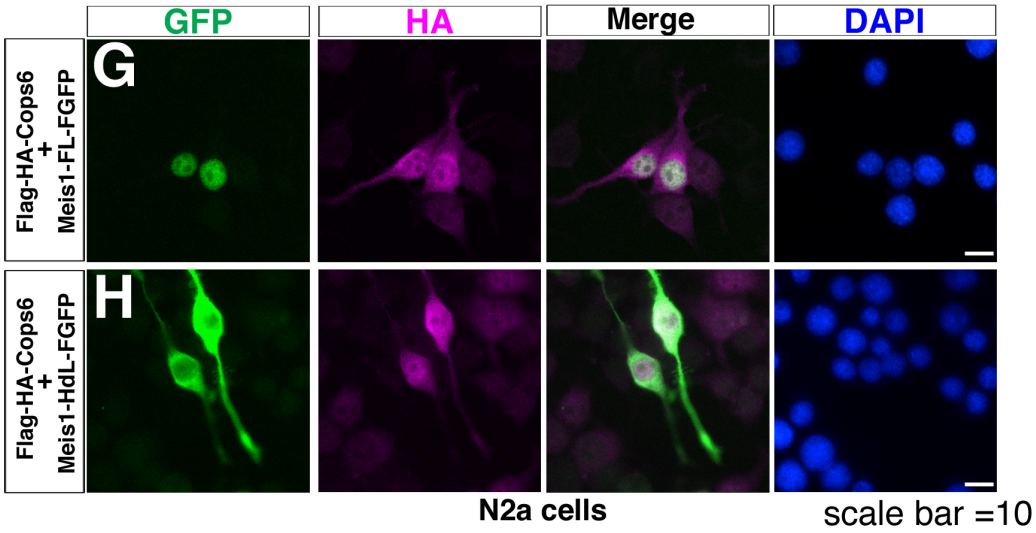
Figure 6-figure supplement 1